July 2020

Study on the Chemical and Mechanical Stability of Polymer Nanofluidic Biosensors

Dae Won Kim

STUDY ON THE CHEMICAL AND MECHANICAL STABILITY OF POLYMER NANOFLUIDIC BIOSENSORS

A Thesis

Before Submitted to the Graduate Faculty of the
Louisiana State University and
Agricultural and Mechanical College
in partial fulfillment of the
requirements for the degree of
Master of Science in Mechanical Engineering

in

The Department of Mechanical Engineering

by
Dae Won Kim
B.S. Sunmoon University, Korea, 2017
Spring 2020

ACKNOWLEDGMENTS

I would first like to thank my faculty advisor Dr. Sunggook Park for his warmest support, invaluable guidance, and insightful discussions throughout my graduate studies. His expertise as a researcher and instructor has helped me become a better communicator, a more innovative researcher, and an effective engineer. I would also like to thank Dr. Junseo Choi for all of his advice and affection. I sincerely felt assured with him not only educationally, but also personally. Finally, I would like to thank Dr. Dorel Moldovan and Dr. Manas Gartia for agreeing to serve on my advisory committee.

I thank the P41 Center for BioModular Multiscale Systems for Precision Medicine (P41EB020594) from the National Institutes of Health for sponsoring this research. I would like to acknowledge Dr. Michael C. Murphy, Dr. Daniel Park, and Dr. Steven Soper for their collaboration in this project offering valuable input. I would also like to thank all the members of my research group: Ramin Riahipour, Qinhan Liu, Yijie Kang, and Dr. XiaoXiao Zhao for their research support and assistance.

Besides, I would like to thank Young-Ho Shin, Jongyoon Park, Bomi Hwang, Sujie Park and Jeong Tae Ok for their psychological support and affection, and Steven Williams, Austin Saizan, and Jonah Carpenter for their English writing support. I was able to overcome hardships with their advice and help.

Finally, I give my deepest gratitude to my family for their unyielding support and inspiration from which I have drawn the strength and perseverance to overcome many challenges. Thank you for being there every step of the way.

Table of Contents

ABSTRACT

Polymer nanofluidic devices have great potential to replace silicon (Si) and glass-based nanofluidic devices in biomedical applications due to their advantages such as low material and fabrication cost, various physicochemical properties, well-developed surface modification protocol, and low electrical noises for electrical measurements. In nanofluidic sensing applications, single molecules such as DNA are introduced into the fabricated nanochannel or nanopore, measuring their physicochemical properties optically or electrically. The properties of materials for nanofluidic devices have a significant role in the performance of the devices, such as DNA translocation and device stability.

Among several nanoscale fluidic physics, surface charge density is a key material property of nanofluidic devices related to the capture of single molecules because it determines the magnitude of electrophoresis and electroosmosis in the nanostructures. To facilitate the capture of single molecules into nanofluidic devices, polymers containing poly(ethylene glycol) (PEG) are preferred due to their low surface charge density and reduction of surface fouling of biomolecules. However, a drawback of PEG-based polymers is a weak chemical and mechanical stability due to swelling effect and low surface hardness when in contact with electrolytes.

This work presents an improvement in the chemical and mechanical stability of a nanofluidic device formed in poly(ethylene glycol) diacrylate (PEGDA), a PEG-based UV resin for UV-NIL, by adding a cross-linking agent (e.g. TMPTA). First, we defined the surface charge density of polymers such as PMMA, COC 6013, and PEGDA with the different O_2 treatment time because these three polymers have low surface charge density compared to other polymers. Then, we studied the effect of the cross-linking agent content on the surface charge density of PEGDA-TMPTA material and on the translocation of DNA molecules through the nanopore. Five different compositions of PEGDA resins with varied amounts of a cross-linking

agent, trimethylolpropane triacrylate (TMPTA), were used (pure PEGDA, ratio 5:1, 1:1, 1:2, and 1:5). The surface hardness of PEGDA-TMPTA resin increases according to the crosslinking agent concentration from 139 MPa (pure PEGDA resin) to 205 MPa (1:5 resin). To be specific, the surface hardnesses of pure PEGDA, 5:1, 1:1, 1:2, and 1:5 were 139 MPa, 158 MPa, 196 GPa, 204 MPa, and 205 MPa, respectively. The surface charge densities at 0.001M KCl (pH 8.0) of pure PEGDA, 5:1, 2:1, 1:1, and 1:5 were $-9.5 \pm 0.09\, mC/m^2$, $-7.9 \pm 0.97\, mC/m^2$, $-7.1 \pm 1.06\, mC/m^2$, $-7.5 \pm 1.10\, mC/m^2$, and $-7.4 \pm 0.57\, mC/m^2$, respectively. These observed surface charge densities of PEGDA-TMPTA resin exhibit a decreasing trend which is beneficial for DNA translocation into nanostructures. In conclusion, this approach has a positive influence on the chemical and mechanical stability of nanofluidic devices concerning DNA translocation into a nanopore or a nanochannel.

CHAPTER 1. INTRODUCTION

1.1. General Background

Undoubtedly, healthcare plays a significant role in modern society. To be specific, “Precision Medicine”, which refers to novel diagnostics targeted for patients based on their genetic characteristics, has been a vital part of healthcare in recent years [1]. This approach will assist engineers and doctors to predict more accurately which treatment and prevention strategies for a particular disease, especially cancer, will work in which groups of people. Cancer can be distinguished by using genetic information, and therefore genetic information by DNA sequencing is the key to success. However, fundamental DNA sequencing such as Torrent sequencing and Illumina sequencing faces limitations on the high replication cost as well as the speed at which target molecules can be detected [2]. When it comes to a faster and cheaper sequencing platform, nanofluidic biosensors having nanoscale detecting areas are a great tool for performing DNA sequencing by taking advantage of their smaller geometry of the sensing area and the cost-effectiveness of materials requirements [3, 4].

DNA sequencing methods currently on the field can be mainly classified into the non-nanopore method and the nanopore-based method [5]. The non-nanopore DNA sequencing method requires a lot of sample preparation and complicated algorithms for data processing, while the nanopore-based DNA sequencing method can be performed using a relatively straightforward method with significant benefits such as label-free, ultra-long reads (10^4-10^6 bases), high throughput, and low material requirement. To be specific, a nanoscale pore is placed between the inlet and outlet chambers that contain an electrolyte, and voltage is applied across the area inside the nanopore using two electrodes. These conditions lead to a steady stream of ion flow across the pore. Nucleic acid molecules in solution can be driven through the pore, and structural features of the biomolecules are observed as measurable changes in the ion current. The biological information of the DNA molecule can be determined based on the collected ionic current data and the velocity of DNA translocation through a nanostructure.

Nanofluidic biosensors are manufactured by nanofabrication methods. The material used for nanofluidic biosensors during nanofabrication is a critical parameter in terms of their functionality and application. Consequently, nanofluidic biosensors can be assorted into mainly two groups such as inorganic-based nanofluidic sensors (e.g. Si or glass-based) and organic-based nanofluidic sensors (e.g. polymer-based). Inorganic-based nanofluidic sensors are known for low flexibility, electrical conductivity, and nonflammability, while organic-based nanofluidic sensors are known for the high melting point, boiling point, and low electrical conductivity [6]. Therefore, we need to manipulate and optimize nanofluidic devices for fabrication purposes, using organic-based polymer. As shown above, there is a critical weakness of organic-based nanofluidic devices, namely short device stability for the long-term electrical measurement. To overcome that drawback, in this work we will present methods to improve the chemical and mechanical stabilities of polymer-based nanofluidic biosensors for DNA sequencing.

1.2. Goals and objectives

The goal of this thesis is to develop material properties with regards to the stability of polymer-based nanofluidic devices for long-term usage. Polymers play a significant role in the performance of nanofluidic devices when it comes to optimizing the device functionality. Polymers have a lot of advantages including non-toxicity, cost-effectivity, electrical properties in the improvement of biosensing systems, and low electrical noises for electrical measurement. It is necessary to use their advantages to achieve successful fabrications and more effectively translocate DNA molecules into nanostructures such as nanopores, nanoslits, and nanochannels. Firstly, three most-used polymers (impact-modified PMMA, COC 6013, and PEGDA) for nanofluidic biosensors are focused in this study to define their surface properties including zeta potential and surface charge density in diverse conditions, such as O_2 treatment and aging time in the air. We measured the zeta potential and surface charge densities of these three polymers utilizing through SurPASS 3 zeta potential measurement machine (Anton Paar). After the measurement, it turns out that PEGDA is the best option for the flatform of our nanofluidic biosensor. However, the critical problem is that PEGDA has poor chemical stability. Thus, we use a crosslinking agent to improve the chemical stability of PEGDA. By adding a crosslinking agent (e.g. TMPTA), we resolve this critical problem from PEGDA and we can better take advantage of its beneficial properties.

There are three core objectives for this study: the first objective is to define zeta potential and surface charge density for optimizing nanofluidic devices, the second objective is to improve the chemical stability of nanofluidic devices, and the third objective is to improve the mechanical stability of polymer-based nanofluidic devices.

1.3. Outline of the manuscript

There are five chapters in this thesis and the concise summary of each chapter is given below.

Chapter 1 covers a purview of this thesis and the goal and objectives of this study.

Chapter 2 shows the literature review on topics within the key description of the biosensing research project in nanofluidic devices.

Chapter 3 focuses on the zeta potential (ζ) and surface charge density (σ) for polymer in biosensor nanofluidic devices. The trend of the zeta potential and surface charge density according to the amount of the O_2 treatment time and aging time in the air.

Chapter 4 demonstrates the effect of crosslinking agents (TMPTA) on PEGDA which is an ultraviolet resin for nanoimprint lithography. This chapter shows that crosslinked PEGDA resin has different material properties which are critical factors for nanofluidic devices such as surface charge density, surface hardness, and the velocity of DNA translocation through nanopore or nanochannel. The trend of properties of PEGDA resin according to the concentration of crosslinking agent and effect will be covered in this chapter.

Chapter 5 provides a conclusion to the key descriptions focused on this research as well as an outline for future work.

CHAPTER 2. LITERATURE REVIEW

This chapter will review the literature that is related to the scope of polymer-based nanofluidic biosensors. First of all, the physics of nanoscale fluidics will be introduced, followed by a summary of the core principles and advantages of polymer-based nanofluidic biosensors. Next, the overall concept of zeta potential and surface charge density in polymer-based substrates will be reviewed with a focus on nanofluidic biosensors. Subsequently, relevant work on measuring zeta potential and surface charge density will be described. Thirdly, the fabrication of nanofluidic devices in plastic will be covered, followed by requirements for materials to be used for nanofluidic applications such as UV-resin. Lastly, the effects and advantages of a crosslinking agent on a plastic substrate for nanofluidic devices will be reviewed.

2.1. Polymer-based nanofluidic biosensors

2.1.1 Physics of nanoscale fluidics

Nanofluidic systems are defined as systems with functional or critical dimensions of structures in the 1-100 nm range [7, 8]. In recent years, the interest in nanofluidics-based sensing targeting single molecules has grown. This sensing technique requires at least one characteristic dimension of the confined channel below 100 nm. The main transport phenomena in nanofluidic systems can still be explained by a hypothesis based on the continuum and mean-field approaches. Three parameters in this system play significant roles in the transport of solutes and solvent passing through nanochannels or nanopores: the presence of external forces, electrokinetic forces, electrical forces between a charged wall and solute molecules, and friction forces between a wall and a solvent. Based on these forces, electrokinetic phenomena in the nanofluidic systems can be divided into four groups shown in Figure 2.1. The four groups include:

- *Electroosmosis* is referred to as the flow of liquid related to a stationary charged surface. This electroosmotic flow depends on the properties of a charged surface [9].
- *Electrophoresis* is defined as the flow of a charged surface, technically charged particles, related to a stationary fluid under the influence of an electric field. Different charge-to-mass (q/m) ratio of the charged particles results in the separation of particles into discrete areas as a function of q/m ratio [10].
- *Streaming potential* is referred to as the induced electric field made up of the liquid carrying away the ions with the charge opposite to the surface when ionic solutions flow along with external forces. This potential is the opposite concept of electroosmosis [11].
- *Sedimentation potential* is defined as the induced electric field when charged particles flow along with a stationary fluid. This potential is the opposite concept of electrophoresis [12].

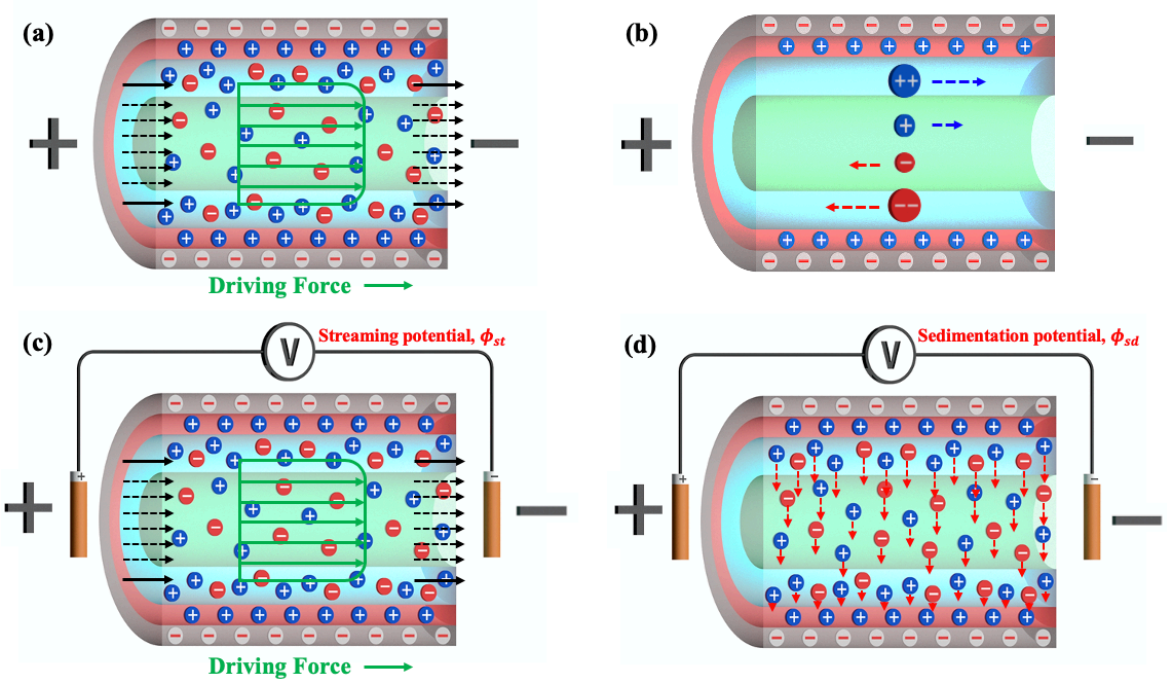

Figure 2.1. Schematics of electrokinetic phenomena in a negatively charged nanochannel: (a) electroosmosis, the flow generated by the movement of the stern layers under the electrofluidic field; (b) electrophoresis, the inherent movement of charged ions towards the attractive electrode; (c) streaming potential, the induced electric field by the electroosmosis flow; and (d) sedimentation potential, the electrical potential generated by the movement of charged ions settled by the gravitational force.

There are several applications based on these four nanofluidic phenomena. Lee *et al.* suggest that the electroosmosis can be improved, reduced, eliminated, and even reversed utilizing through an external electric field to govern the zeta potential at the aqueous capillary interface [13]. They developed a technique to enhance separation resolution and to halt protein adsorption by applying an external electrical potential to affect the potential inside the capillary. The absolute value of the zeta potential increased from -29 mV without an external potential to – 35 mV with a -5 kV potential gradient. However, the polarity of the zeta potential can be inverted at + 6 kV potential gradient. Jorgenson *et al.* defined the zone electrophoresis in open tubular capillaries [14]. Based on their results, this technique was found to be a useful tool for high-resolution separations of charged substances with the help of heat transfer from small-diameter capillaries. They developed an instrumental format for zone electrophoresis utilizing a sample injection technique and on-line zone detection. Leung *et al*. utilized streaming potential measurements to detect the existence of adsorbed polyvinylamine or potassium polyvinylsulfate in paper-based microfluidic devices [15]. They performed the streaming potential measurement to provide an electrical interface for paper-based sensors. The measured potentials were obtained from a capillary-driven flow in a filter paper and the range is between −80 and +80 mV. The magnitude and polarity of the measured potentials were sensitive to the presence of adsorbed polymer. They claimed that streaming potential may generate an electronic interface for paper-based biosensors. Saville researched on a gradient of electric potential formed by sedimentation of charged particles immersed in an electrolytes [16]. He described that the influence of the potential field around a single particle on the sedimentation velocity becomes significant when the double layer is thick. Variations in the sedimentation coefficient, which is the ratio of the sedimentation velocity of a particle, are also reflected in the Brownian diffusivity of suspended particles but here the effect appears less significant.

2.1.2 Polymer-based nanofluidic devices

In the recent past, the majority of researches utilizing nanofluidics have focused on using glass, fused silica or silicon (Si) as the substrate material of the devices to take their advantage such as established surface chemistry, excellent optical properties, well-established fabrication technologies, and maintainability during the thermal or pressure processing. However, these inorganic-based nanofluidic devices have critical defects. The defects are extensive device preparation steps and high-fabrication costs. Therefore, polymers can be an attractive alternative to inorganic-based materials for nanofluidic biosensors due to their diverse range of physicochemical properties, low material cost, a variety of surface modification protocols that can be used and several fabrication techniques.

There are two general categories of polymeric materials that have been used for nanofluidic devices: (1) elastomers and (2) thermoplastics. Elastomers are unstructured polymers with a few cross-links between polymer chains. While the low Young's modulus enables large deformation upon application of an external load, covalent cross-links help elastomers return to their original shape upon release of the load. Polydimethylsiloxane, PDMS, is a good example of an elastomeric material. On the other hand, thermoplastics are usually linear or branched polymers with higher molecular weights and Young's modulus. Examples of thermoplastics are poly(methyl methacrylate), PMMA; polycarbonate, PC; and cyclo-olefincopolymer, COC. Some of the physiochemical properties of common polymers used for nanofluidics are shown in Table 1.

Table 1. The physicochemical properties of common polymers and comparison to glass [17]

Material	Acronym	T_g/°C	T_m/°C	CTE (α) ppm °C^{-1}	Refractive index	Young's modulus/GPa	Optical transmissivity	
							UV	Vis
Polystyrene	PS	92–100	240–260	10–150	1.55–1.59	3.3–3.5	Poor	Excellent
Polycarbonate	PC	145–148	260–270	60–70	1.584	2.0–2.4	Poor	Excellent
Poly(methyl methacrylate)	PMMA	100–122	250–260	70–150	1.492	1.8–3.1	Good	Excellent
Cyclic olefin co(polymer)	COC	70–155	190–320	60–80	1.53	2.6–3.2	Excellent	Excellent
Poly(ethylene terephthalate)	PET	69–78	248–260	48–78	1.575	2.0–2.7	Good	Good
Polypropylene	PP	−20	160	18–185	1.49	1.5–2.0	Fair	Good
Poly(dimethylsiloxane)	PDMS	−125	−55	67.3	1.40	0.36–0.87 × 10^{-3}	Excellent	Excellent
Glass (Soda lime)	G	520–600	1040	9	1.52	50–90	Good	Excellent

CTE—Coefficient of thermal expansion (linear).

When it comes to utilizing the properties of diverse polymers, material selection is the key point of regulating the fabrication cost and determining device functions. When materials are chosen, compatibility with operating conditions and operating purposes must be considered. Different materials can result in different fabrication processes. In opposition to this cause and effect, material selection can be reversely limited by the fabrication strategy depending on the application. Therefore, it is necessary to evaluate the most efficient material for target fabrication. When modified by certain chemical treatments, the surface of polymer materials can also exhibit rich surface charges and/or specific functional groups that can be beneficial for many applications in nanofluidic fields. However, polymers often have low values of both Young's moduli and interfacial free energy. This can pose a major concern, possibly causing stress or affinity induced channel collapses or unstable surface properties (hydrophobicity recovery), especially during the thermal bonding or demolding process. We will study a fascinating solution to this issue in the following chapters.

For the past years, the polymer-based nanofluidic biosensor field has dramatically developed due to the trend of health care including genetically related diseases, especially cancer, and medical treatment. With the rapid development of the nanofluidic biosensor, nanoscale structures enhance the accuracy of DNA detecting sensors with the help of compacted detecting area [18], and also improve surface binding reactions because the target molecules are closely confined to the surfaces that are coated with specific binding sites [19]. Schoch et al. demonstrated that the detection of analytes in nanochannels with an applied convective flow through the channels has a positive effect on diffusion-limited reactions, improving the mass transport [20]. This approach shortens the response time to detect targeted molecules due to the fast reaction kinetics in nanofluidic channels. Figure 2.2 indicates the design of Schoch's device using nanochannels for electrical sensing of biomolecules.

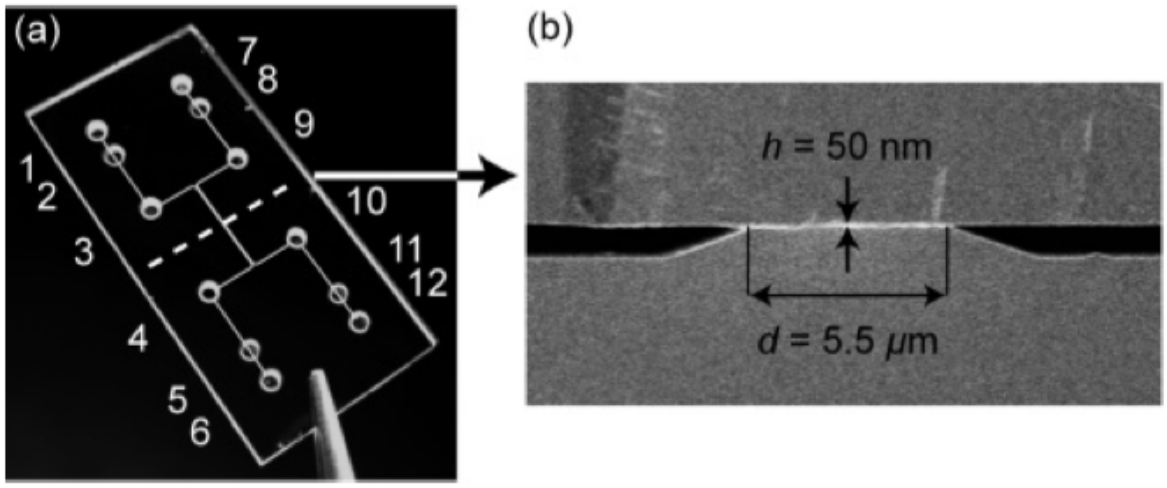

Figure 2.2. Design of the device, consisting of two microchannels joined by nanochannels. (a) Photograph of the 12 × 25 mm chip showing the two microchannels and access holes. The cross-sectional view along the dotted line is presented in (b), a scanning electron microscope image showing two microchannels with electrodes at their bottom, which are connected by nanochannels with a height of 50 nm and length of 5.5 μm [20].

2.2. Zeta potential and surface charge density

2.2.1. Introduction of zeta potential and surface charge density.

Zeta potential (ζ) and surface charge density (σ) are impactful parameters in the nanofluidic system because electrokinetic forces in the system can be straightforwardly estimated by these two factors. There are several required concepts to understand zeta potential and surface charge density such as the electric double layer (EDL) and the Debye length. EDL is referred to as two layers caused by the solute concentration distribution near the charged wall of nanochannels or nanopores, increased concentration of counter-ions, and decreased concentration of co-ions adjacent to the wall. Therefore, EDL is one of the important factors in nanofluidic systems. The electrical double layer consists of two layers that include ions and charged particles. The first surface layer of counterions is the Stern layer which is considered to be an immobile layer. The second layer is called the shear plane and is mobile relative to the first Stern layer, and the potential at the shear plane is defined as the zeta potential (ζ). When colloidal charged particles are separated in a medium containing free charges or ions, the electrostatic interactions are blocked by the free charges. The net double-layer interaction decomposes exponentially with a characteristic length which is called the Debye length (κ^{-1}) [21]. To be specific, the Debye length is the distance from the charged surface where the potential has decayed to the 1/e point or 36.7% of the surface potential. [22, 23]. The Debye length is given by

$$\lambda_D = \left(\frac{\varepsilon_0 \varepsilon_r RT}{2F^c c}\right)^{1/2} \tag{2.1}$$

, where R is the gas constant ($J\ mol^{-1}\ K^{-1}$), ε_0 is the permittivity of vacuum ($F\ m^{-1}$), ε_r is the dielectric constant of the medium, F is the Faraday constant ($C\ m^{-1}$), and T is the temperature (K). λ_D can vary from <1 nm at high ionic strength to a few tens of nm at low

ionic strength. Figure 2.3 shows the schematic of the Debye length, electric double layer (EDL), electrical potential profile from a negatively charged wall [8].

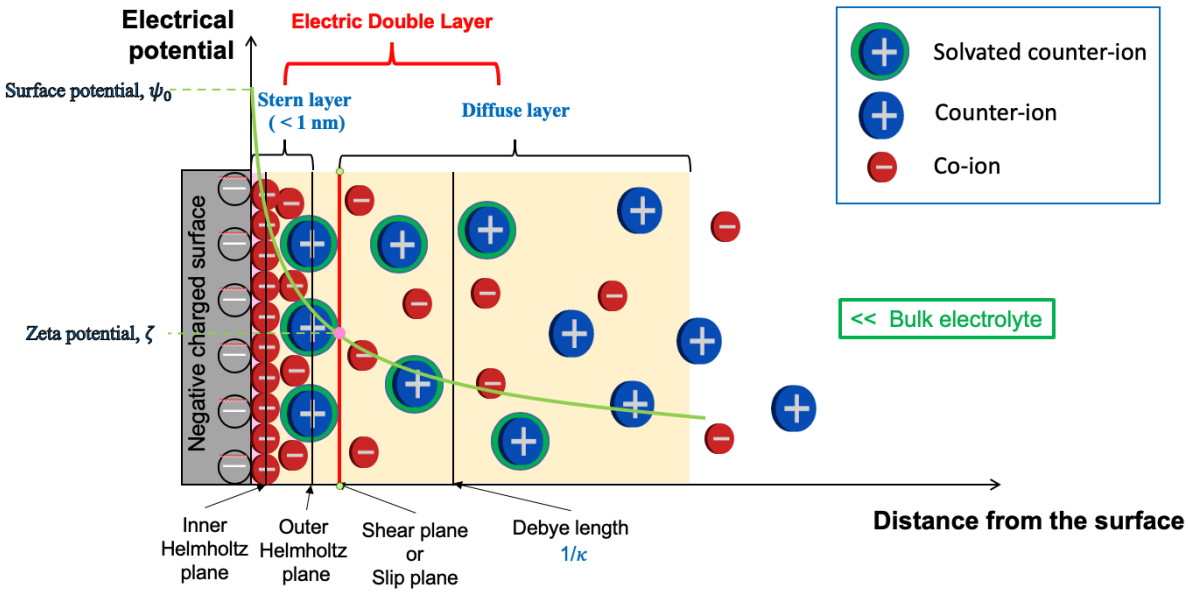

Figure 2.3. Schematic of a Debye length, electric double layer (yellow area), and electric potential profile from the negatively charged wall (Green line)

It is difficult to directly measure the surface charge density during the experiment. Therefore, zeta potential is a critical parameter for nanofluidic devices using a polymer-based substrate because we can evaluate the surface charge density of the material by measuring zeta potential. Furthermore, we can ultimately assess the optimality of the material for the nanofluidic system [24].

2.2.2. Methods to measure zeta potential and surface charge density.

There are two well-known methods to measure zeta potential. The first method is the electroosmosis method. Electroosmotic flow is defined as the flow resulting from the application of an external electric field to a fluid in a microchannel with an ion distribution [25]. This flow will be relatively uniform if the channel dimensions are large compared to the Debye length, and if the channel is homogeneous, straight, and has a uniform surface charge density. The bulk value of the fluid velocity can be then obtained by applying the

Smoluchowski Equation [26], which assumes that the properties of the fluid are uniform and that the non-slip boundary condition applies at the wall of the channel (where $\psi = \zeta$). The fluid velocity is given by

$$u_{EO} = -\frac{\varepsilon\zeta}{\eta}E \tag{2.2}$$

, where ζ is the electrokinetic potential, η is the fluid viscosity, and E is the applied electric field. In turn, the electroosmotic mobility is given by

$$\mu_{EO} = -\frac{\varepsilon\zeta}{\eta} \tag{2.3}$$

The zeta potential is commonly found by measuring the electrostatic mobility, but the exact relationship between zeta and electric potential at the surface is still unclear. We can use Equation 2.4 to form a definition for zeta potential, and it can be assumed that zeta potential is equal to the electrical potential difference between the solution and the interface with the channel wall. Electroosmosis is frequently used to drive flow inside microfluidic channels because for small lengths it can have a greater effect than pressure-driven flow [27].

We can also use streaming current and streaming potential to measure zeta potential [28]. Pressure-driven flow in a microfluidic channel results in the movement of a large number of charges in the fluid. A net electrical current is created when charges are separated at the interface with the channel wall, which creates a net motion of unbalanced charges. The electrical current, or streaming current, is given by [28]

$$I_{stream} = \frac{\varepsilon\zeta}{\eta}\frac{\Delta P}{L}A \tag{2.4}$$

, where A is the cross-sectional area and ΔP is the difference between the upstream and downstream pressures. This equation is specifically for use on channels with circular cross-sections, but it is still a good approximation for channels with geometrically different cross-sections if the double layers are thin compared to the height or radius of the channel and the flow is developed completely. An electric potential can also appear if the current path is not closed during pressure-driven flow. The electrical potential, or streaming potential, is given by

$$\Delta\Phi = \frac{\varepsilon\zeta}{\eta\sigma}\Delta P \tag{2.5}$$

, where σ is the fluid conductivity. This equation uses the Debye-Huckel approximation and assumes a thin EDL limit such that the geometric effects of the channel are insignificant. It is also assumed that the conductivity of the fluid is constant, however, the non-uniform ion distribution and surface conduction may noticeably affect results in small microchannels. The streaming potential is also commonly used to measure zeta potential [29].

In our experiment, zeta potentials for solid materials with a planar surface can be determined using the Helmholtz-Smoluchowski equation [30]. This equation is shown below:

$$\zeta = \frac{dI_{str}}{d\Delta p} \times \frac{\eta}{\varepsilon \times \varepsilon_0} \times \frac{L}{A} \tag{2.6}$$

, where ζ is the electrokinetic potential, η is the fluid viscosity, and $\varepsilon \times \varepsilon_0$ is the dielectric coefficient of the electrolyte solution. For dilute aqueous solutions, the viscosity and dielectric coefficient of water are used. The term $dI_{str}/d\Delta p$ is related to the cell constant of the streaming channel (the gap between adjacent solid samples), L is the length of the rectangular slit channel formed between two planar surfaces, and A is its cross-section (A = W x H) with channel width W and gap height H in Figure 2.4. The below figure shows a schematic representation of the arrangement of solids with planar surfaces and indicates the key dimensions of the streaming channel.

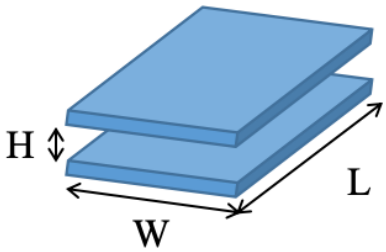

Figure 2.4. schematic figures of the arrangement of solids with planar surfaces

There is an equation that we can define a relationship between zeta potential and surface charge density [28]. Zeta potential is a phenomenological quantity related to the surface charge density for microscale systems. This relationship can be quantified by using the Grahame equation [31]. The surface charge density is given by:

$$\sigma_\zeta = \frac{2\varepsilon_0 \varepsilon_r k_B T}{e\lambda_D} \sinh\left(\frac{e\zeta}{2k_B T}\right) \tag{2.7}$$

, where e is the elementary charge in (C), k_B is the Boltzmann constant in (J/K), ε_0 is the permittivity of the vacuum, ε_r is the dielectric constant of water at 25℃, F is the Faraday constant in (C/mol), T is the temperature of the room in (K), and c is the concentration of KCl in [M]. As shown, the relationship between surface charge density and zeta potential is defined by a non-linear function. It has also been shown that zeta potential can be used to determine the number of isoelectric points on a surface, which provides us with a method to measure changes in ionizable groups on that surface.

Plastic and polymer surfaces are charged and surrounded by the ions with an opposite signal from the electrolytes in the nanofluidic systems. Moreover, the zeta potential has a strong connection to the interactions among the suspending solid particles in an electrolyte, and eventually defines the stability of the suspension solutions. The conventional electrokinetic effect concerning the electro double layer (EDL) at the solid-liquid interfaces is established to control the flow characteristics of electrolytes inside nanostructures [32].

2.2.3. Summary of previous zeta potential results for typical polymer substrates

There are several previously recorded sets of data for the zeta potentials of other polymers. These results can be used to observe the natural trends of the zeta potentials of different polymer materials concerning pH. Zeta potential results were reported in terms of ζ /pC vs. pH and ζ vs. pC. As opposed to pH, "pC" is defined as the negative logarithm of the counterion concentration. It is given by the equation:

$$pC = -\log c \tag{2.8}$$

, where c is the concentration of the counterion. The pC is then related to the zeta potential as follows:

$$\zeta = a_0 + a_1 pC \tag{2.9}$$

Table 2.1. shows that summarized zeta potential values for typical polymers such as PMMA, PC, PDMS, and PET.

Table 2.1. Summary of previous zeta potential measurement for polymers [33-35].

Material	Method	Measurement Conditions	Zeta potential (ζ)	Reference
PMMA Polymethylmethacrylate	1) EOM (Electroosmotic mobility) 2) Subablation fluences from pulsed lasers have been used to modify zeta potential (ζ)	Counterion: Na+/K+ Buffer ion: Acetate, borate (a) ζ /pC vs. pH for PMMA. (b) ζ vs. pC for PMMA. (7 < pH < 8)	Figure 2.5.	A [36], B [37], C [38], D [39], E [40]
PC Polycarbonate	EOM (Electroosmotic mobility)	Counterion: Na+/K+a Buffer ion: Carbonate (a) ζ /pC vs. pH for PC. (b) ζ vs. pC for PC. (6.8 < pH < 7.2)	Figure 2.6.	A [38], B [39], [41], C [42], D [43], E [44]
PDMS Polydimethylsiloxane	1) EOM (Electroosmotic mobility) 2) Plasma-oxidation and polyelectrolytes	Counterion: K+ Buffer ion: Phosphate (a) ζ /pC vs. pH for PDMS. (b) ζ vs. pC for PDMS. (6.5 < pH < 7)	Figure 2.7.	A [41], [45], B [38] C [46], D [26], E [47], F [48]
PET Polythylene terephthalate	1) EOM (Electroosmotic mobility) 2) Alkaline hydrolysis	Counterion: Na+/K+a Buffer ion: Phosphate (a) ζ /pC vs. pH for PET	Figure 2.8.	A [37], B [42], C [43], [49], D [50], E [51]

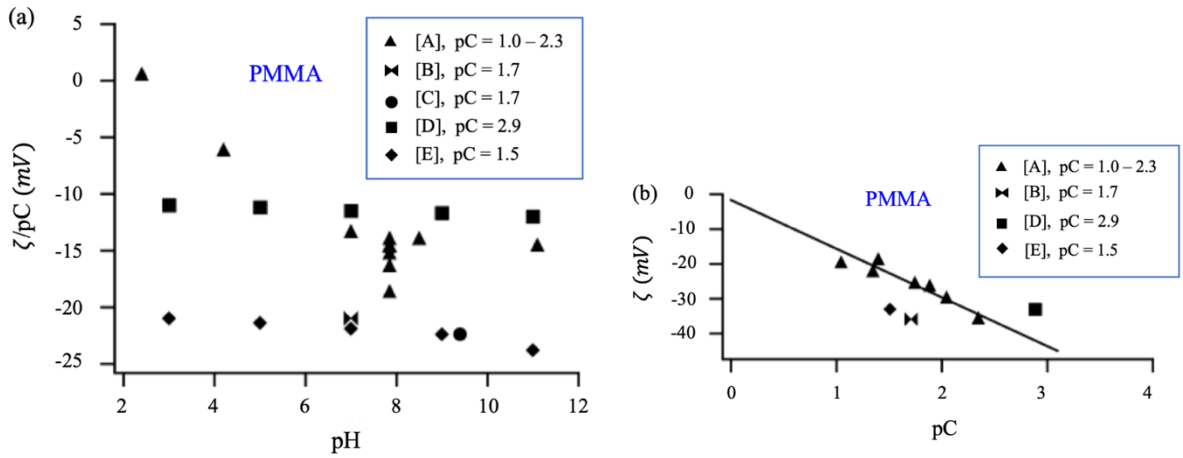

Figure 2.5. Combined plot of previous zeta potential measurement for Polymethylmethacrylate (PMMA). Electroosmotic mobility was used and sub-ablation fluences from pulsed lasers were used to modify the zeta potential. Measurements were taken using Na+/K+ as the counterion and acetate/borate as the buffer ion. ζ vs. pC results were given for a pH range of 7 to 8 [33].

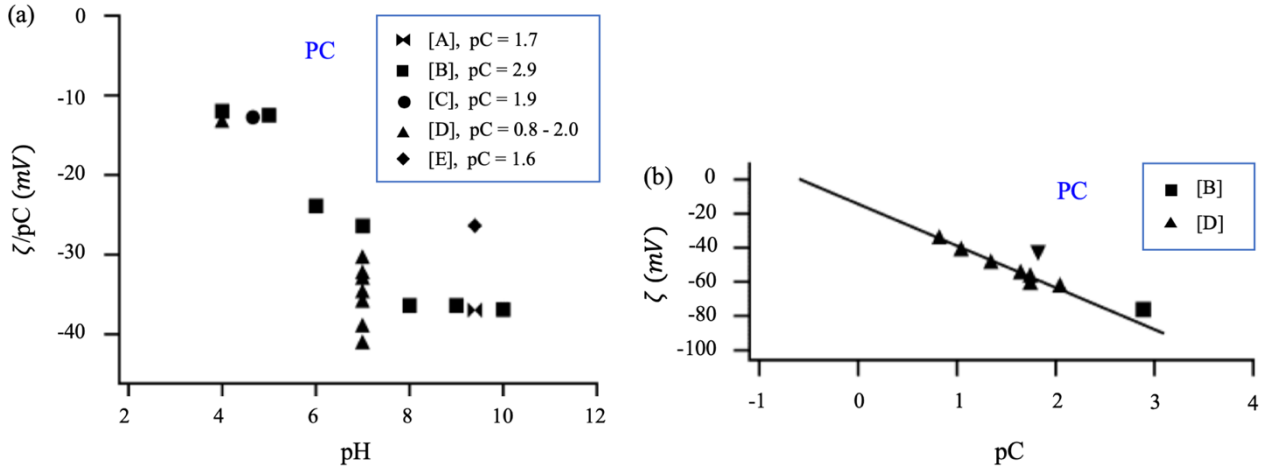

Figure 2.6. Summary of previous zeta potential measurement for polycarbonate (PC). electroosmotic mobility was used to modify the zeta potential. The counterion used was Na+/K+ and the buffer ion used was carbonate. ζ vs. pC results were given for a pH range of 7 to 8.

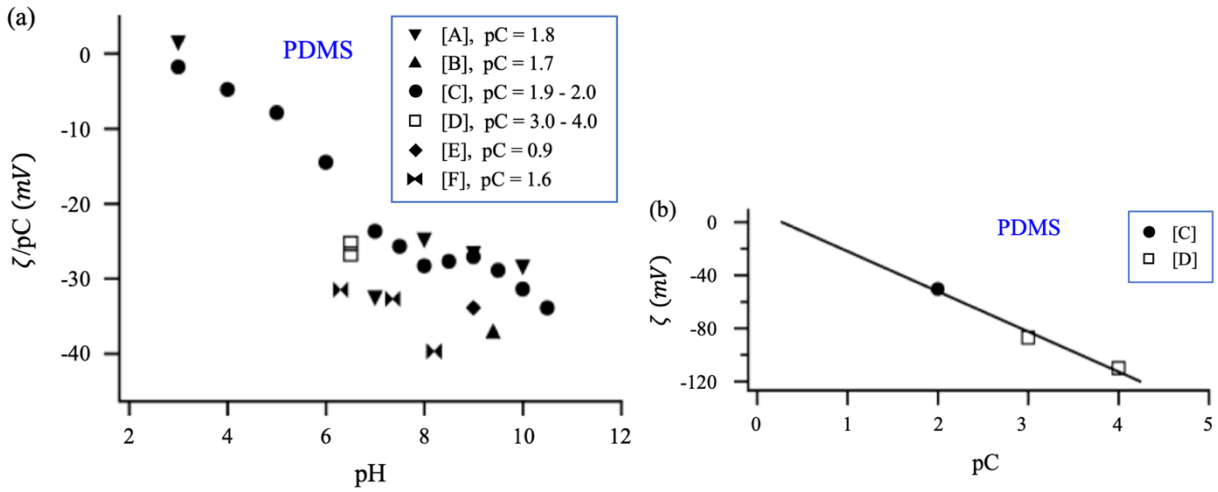

Figure 2.7. Summary of previous zeta potential measurements for PDMS. Electroosmotic mobility, polyelectrolytes, and plasma-oxidation were used. The counterion used was K+ and the buffer ion used was phosphate. ζ vs. pC results were given for a pH range of 6.6 to 7 [41].

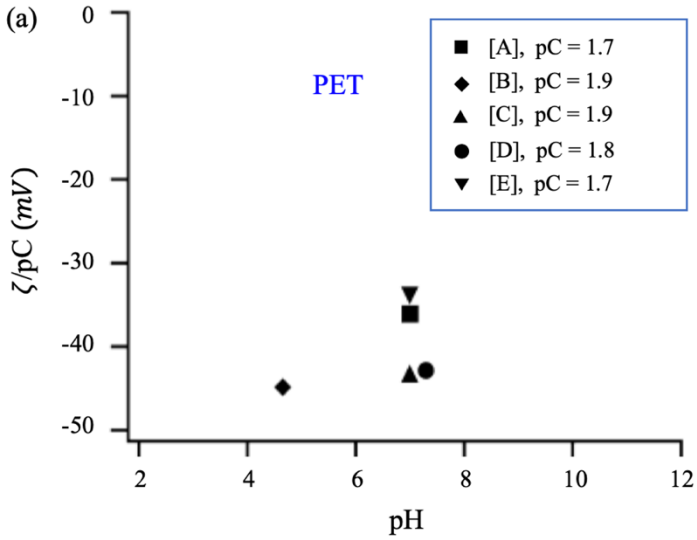

Figure 2.8. Summary of previous zeta potential measurements for PET. Electroosmotic mobility and alkaline hydrolysis were used. Na+/K+ was used as the counterion and phosphate was used as the buffer ion [49, 50].

2.3. Fabrication of polymer-based nanofluidic devices.

The major differences of polymer-based nanofluidic devices from glass nanofluidic devices is the ability to perform the nano-replication to directly produce the prerequisite structures and also assemble devices, where the assembly consists of enclosing the fluidic network using thermal fusion bonding with a temperature close to the material's glass transition temperature (T_g). Tons of practical nanofabrication skills for polymer-based nanofluidic devices have developed for a few decades such as photolithography, hot embossing lithography, and injection molding [52]. However, we will focus on the nanoimprint lithography (NIL) for organic-based nanofluidic biosensors in this chapter, firstly describing prerequisite fabrications for NIL.

2.3.1. Prerequired process for NIL: Electron beam lithography (EBL) and Focused Ion Beam (FIB)

Electron beam lithography (EBL) is a nanofabrication process utilizing a focused electron beam to form tiny structures in the resist. These structures are then used to pattern the substrate through reactive ion etching (RIE) or other etching/deposition processes. However, unlike conventional lithography, EBL creates a pattern directly in the resist without the need for masks. The process of electron beam lithography is illustrated in Figure 2.9.

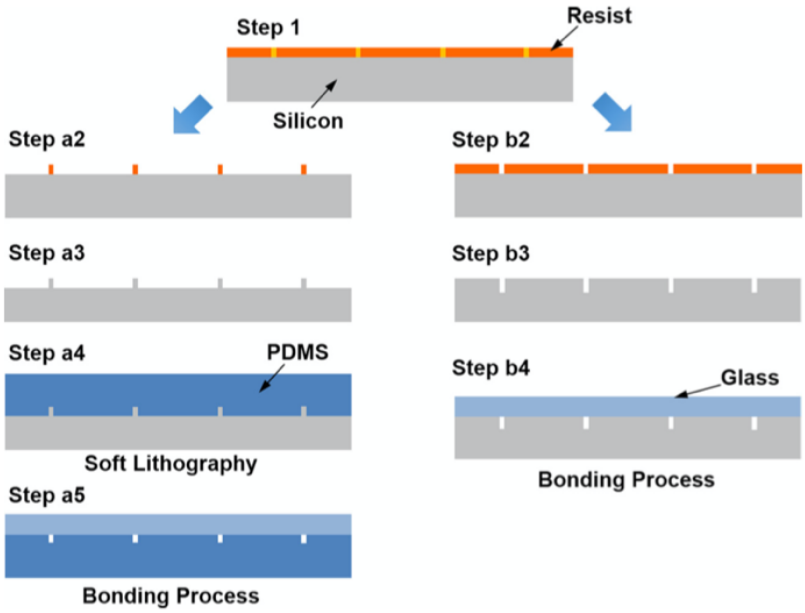

Figure 2.9. Schematic of electron beam lithography. First, the resist is exposed to an electron beam. Then, either negative (a) or positive (b) resist patterning is used [52].

The second skill in this area is Focused Ion Beam. This technique utilizes a focused beam of ions to improve the accuracy of fabrications on the substrate. FIB is known as an impactful defect-repair tool in a semiconductor manufacturing. In the past few years, the attention to FIB milling has dramatically increased in the nanofabrication because it is efficient and effective to fabricate precise nanoscale patterns directly on hard substrates without masks or photoresists. The process of electron beam lithography is illustrated in Figure 2.10.

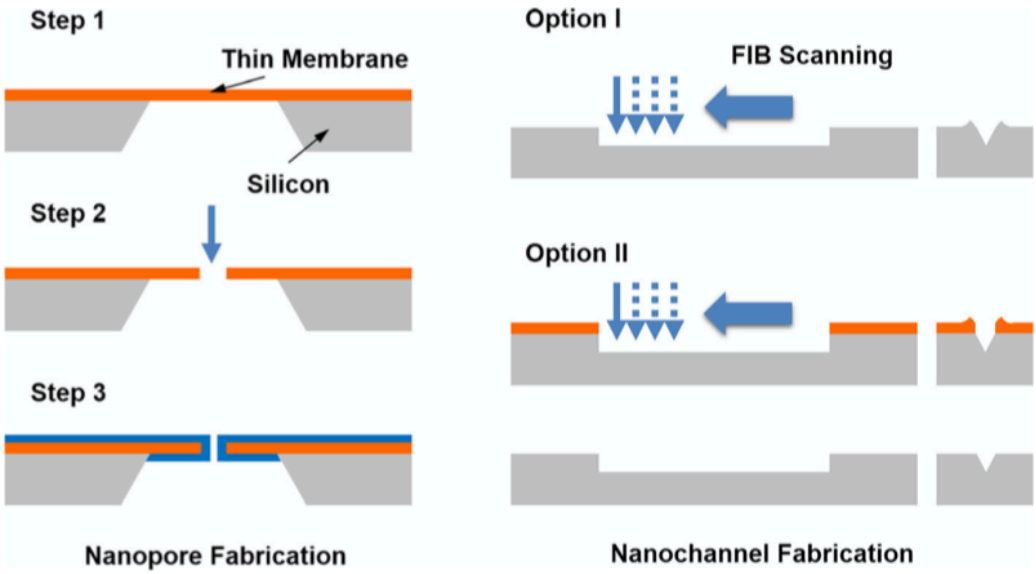

Figure 2.10. Schematic of nanopore/nanochannel focused ion beam methodology. Nanopore fabrication: A thin membrane is deposited and a back chamber is etched, followed by FIB milling. The nanopore is then shrunk using an isotropic deposition. Nanochannel fabrication: Option (I) utilizes Direct FIB scanning. Option (II) utilizes the deposition of a sacrificial layer, followed by FIB scanning and sacrificial layer etching. This additional sacrificial layer can remove imperfections or ridges that formed during FIB scanning [52].

2.3.2. Nanoimprint lithography (NIL)

Unlike these two lithography methods which fabricate nanoscale patterns on the substrate, Nanoimprint lithography (NIL) is a practical nanolithography method that can replicate nanoscale features by mechanically pressing pre-established molds into imprint resist [53]. There are two main sub-parts of NIL. One is thermal-NIL which adjusts heat to make patterns on substrates based on the glass transition temperature (T_g) of the substrates, and the other one is ultraviolet (UV)-NIL which utilizes UV resist that can be solidified by UV light. The fabrication processes of thermal-NIL and UV-NIL are shown in Figure 2.11. By utilizing the diversity of applications in a specific situation, this method has been used to overcomes the diffraction limit during nanofabrication. Especially, it has been widely used in recent decades to fabricate 1-D and 2-D nanochannels in varied nanofluidic systems.

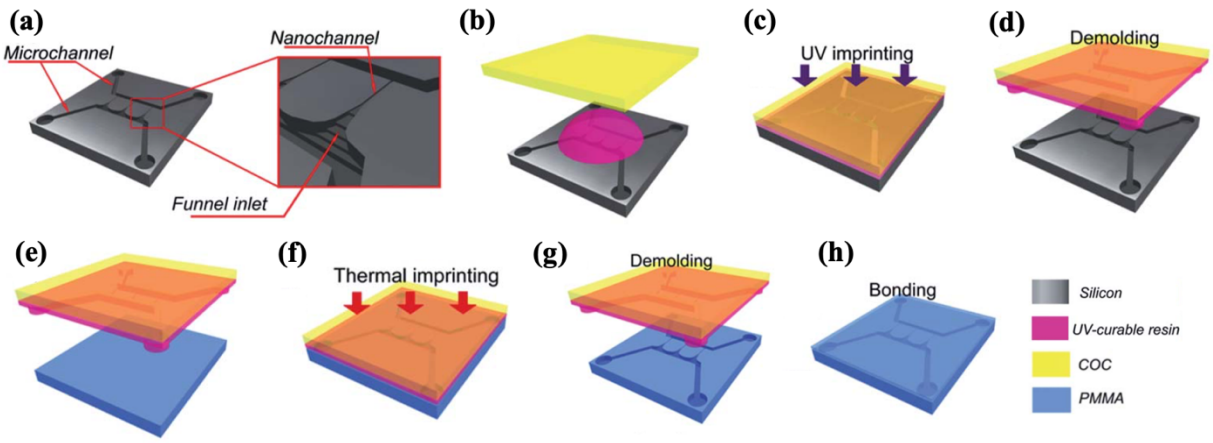

Figure 2.11. Schematic of the design and fabrication processes for the polymer-based nanofluidic device. (a) Silicon master, which consisted of micron-scale transport channels and a funnel-like inlet for the nanochannels; (b)–(d) fabrication steps to produce a protrusive polymer stamp in a UV-curable resin by imprinting from the silicon master; (e)–(g) fabrication steps to generate nanofluidic structures in PMMA by imprinting from the UV-curable resin stamp; (h) bonding step with a PMMA cover sheet to build the enclosed mixed-scale polymer device with microchannels and nanochannels [54].

In the NIL process, the functionality of molds is a critical factor for the resolution of nanopatterns. For example, Choi *et al.* developed an effective process for the fabrication of polymeric dual-scale nanoimprinting molds [55]. They make use of the thin flexible SU-8 stencil membrane as a mold material that can be utilized by UV-NIL. Figure 2.12 shows the entire process of the fabrication for the UV-resin membrane having dual-scale perforated structures. Consequently, they insist the freestanding membrane has a strong potential of usage for a substrate of surface plasmon resonance sensors. In this regard to membrane technology, there is an effecttive method to fabricate desire pore size during imprinting.

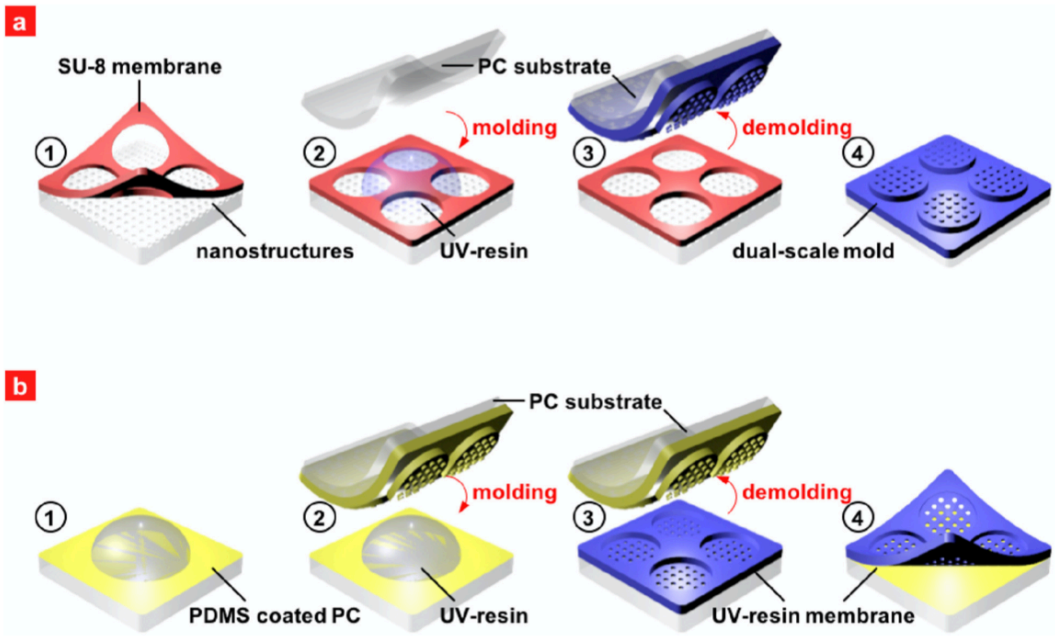

Figure 2.13. (a) Schematics of fabricating dual-scale nanoimprint molds: place a piece of SU-8 membranes over a nanostructured substrate. Then, treat with a thin PDMS layer or a fluorinated silane (1); dispense drops of UV-curable resin and slightly press with a flexible PC substrate. Then, expose to flash-type UV-light (2); peel off the UV-cured sample (3); and coat a thin PDMS layer on the UV-cured sample for self-replicating (4). (b) Schematics of fabricating UV-resin freestanding membranes having dual-scale perforated structures: dispense drops of UV-curable resin on a PC substrate coated with the thin PDMS layer (1); slightly press with the UV-resin mold self-replicated from the UV-resin master and coated with the thin PDMS layer. Then, expose to flash-type UV-light (2); peel off the UV-resin mold (3); and gently peel off the UV-cured membrane from the PC substrate (4) [55].

Also, the high-end nanofabrication tools such as EBL and FIB can be skipped by using NIL. For example, Choi *et al* create perforated micro/nanopore membranes utilizing through UV-NIL and pressed self-perfection process (PSP) for reducing pore sizes [56]. To sum up, they make it possible to reduce pore diameter significantly by applying pressure at an elevated temperature through the reflow of the uncured SU-8. SEM images of the cross-sectional area of micro-scale pore and trench, and result of final pore size as a function of process time shown in Figure 2.13.

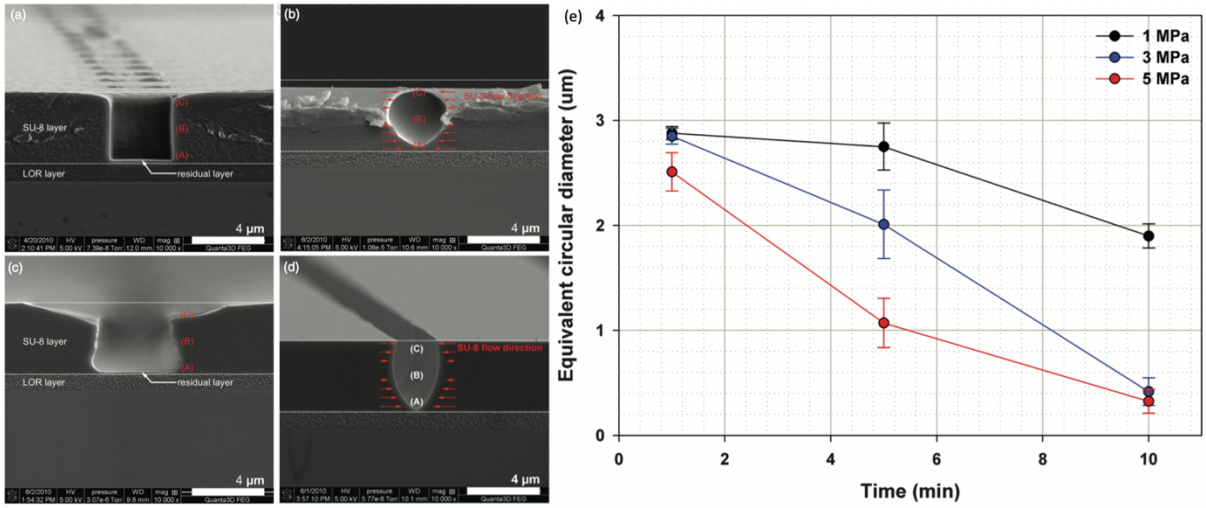

Figure 2.13. SEM images of the cross-sectional area of micro-scale pore and trench: (a), (c) before PSP and (b), (d) after PSP at 55 ˚C, 3 MPa for 10 min. (e) Result of final pore size as a function of process time (with fixed 55 ˚C temperature) for 3.0 μm initial pore, 15 μm period, and 4.0 μm thickness [56].

2.4. Ultraviolet resin for nanoimprint lithography

We need to discuss UV resin in detail because UV-resin can be an attractive alternative to elastomers and thermoplastics. Ultraviolet resin is a specially synthesized polymer that can be solidified by exposure to ultraviolet light and is useful for nano-manufacturing applications [53]. There are two general categories of UV-resin, Positive and negative photoresists. Positive photoresist becomes soluble upon the UV-light exposure because the molecular bindings between monomers are broken by UV-light, while negative photoresist becomes insoluble due to the connected molecular bindings between monomers by UV-light.

One main benefit of using UV-resin as a mold is its excellent demolding property for UV-NIL. Haisma *et al* developed the first UV-NIL paper with the title of Mold assisted nanolithography: a process for reliable pattern replication [57]. This property can be attributed to its thermal expansion coefficient, which is similar to those of polymer substrates, and its low Young's modulus leading to a reduction in the adhesion between the UV-resin mold and the molded substrate. However, a low Young's modulus can also cause the mold structures to deform under high pressure and temperature conditions during thermal-NIL, resulting in a poor replication fidelity in the molded thermoplastic substrate. Thus, Young's modulus of UV-resin molds is required to be high enough to achieve good replication ability during thermal-NIL but at the same time low enough to ensure low demolding force. Another significant advantage of using UV-resin as a substrate is that desired properties, such as surface charge density, can be selectively chosen for nanofluidic fabrications.

A UV resist is made up of a monomer (or oligomer), a cross-linking agent, and a photoinitiator. The monomer is an acryl or epoxy, the cross-linking agent is a molecule with a higher number of functional groups than the monomers, and the photoinitiator is a chemical species capable of initiating the polymerization reaction by activating the functional groups. A

UV-resin can be utilized as both a mold and a substrate. This applicability of a resist to UV-NIL is determined mainly by the chemistry and composition of these three components.

Zheng *et al* reported the replication fidelity of different UV-resin molds copied from a Si master mold via UV nanoimprint lithography (NIL) and their thermal imprinting performance into a thermoplastic polymer. The investigator showed that the replication fidelity among the four UV-resins during UV nanoimprint lithography from a Si master with sharp nanostructures was in the increasing order of (poorest) PUA resin < MD 700 < PPGDA resin < TPGDA resin (best) as shown in Figure 2.14. The results indicate that the high surface energy and small monomer size are keys to achieving good UV-resin filling into sharp nanostructures over the viscosity of the resin solution.

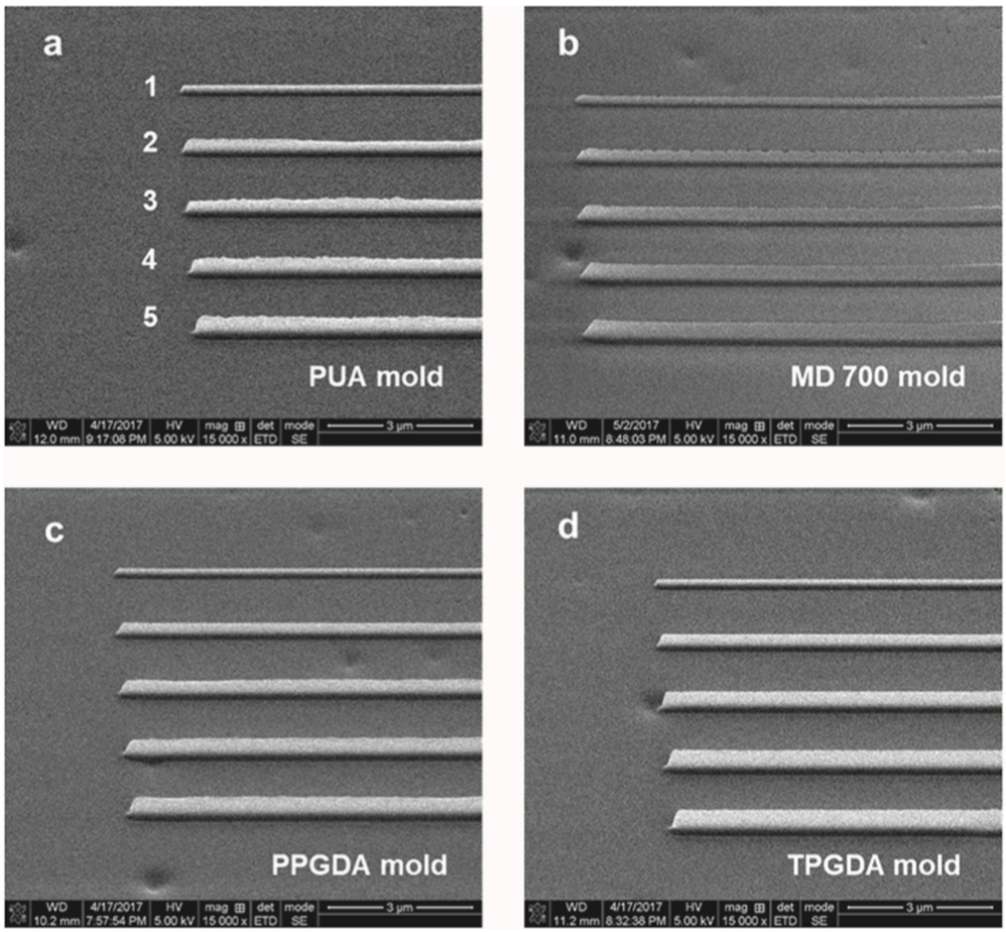

Figure 2.14. SEM images of replicated UV-resin molds by UV-NIL from a Si master. Nanochannel depth increases from top to bottom as indicated by the numbers in the image [58].

Furthermore, Zheng et al. evaluated the electrokinetic surface charge density of nanochannel devices made of different polymers as substrates, such as impact-modified PMMA, COC 6013, and PEGDA [59]. Even though the dimension of five nanochannels of all three devices are the same, the device made up of PEGDA (substrate)-COC 8007 (cover sheet) has a low surface charge density compared to the other two shown in Figure 2.15. This low surface charge density is a key factor for usage in DNA detecting nanopore devices. As shown by Zheng et al, materials with higher surface charge densities than the simulated threshold surface charge potential for a particular nanopore device will not allow DNA to enter the nanopore. Thus, materials with low surface charge densities are considered an attractive choice, as they will be able to facilitate the transfer of DNA or other biopolymers for most any nanopore dimensions and conditions.

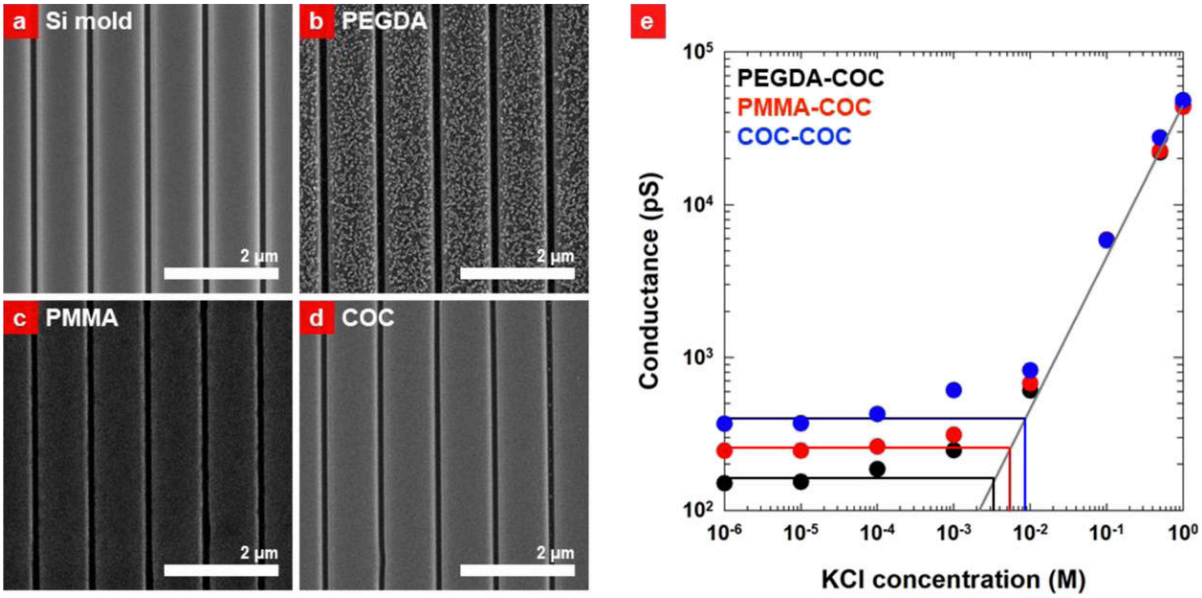

Figure 2.15. SEM images of nanochannel devices for surface charge density calculation and surface charge density calculation results: (a) Si master mold, (b) UV imprinted nanochannels on the PEGDA substrate, (c) thermal imprinted nanochannels on the PMMA substrate, and (d) thermal imprinted nanochannels on the COC substrate. (e) Nanochannel conductance for PEGDA−COC, PMMA−COC, and COC−COC as a function of salt concentration. At high salt concentration, nanochannel conductance is dependent on the bulk solution concentration. At low salt concentration, nanochannel conductance saturates at a value, which is dependent on the surface charge density of nanochannel walls. The transition concentration between these two regimes is indicated in the graph [59].

However, PEGDA has several critical disadvantages for nanofluidic devices application. The disadvantages are its low chemical and mechanical stabilities due to its weak surface hardness and swelling effect. Adding crosslinking agents can be a brilliant solution for the disadvantages of PEGDA. We investigate with regards to adding crosslinking agents into PEGDA in different mixing concentrations in Chapter 4.

2.5. The effect of crosslinking agents on Ultraviolet resin

The crosslinking reaction leads to the formation of insoluble coatings, where polymer chains are joined together to form a three-dimensional network. Extensive crosslinking results in an insoluble and infusible network of linked polymer chains [60]. Covalent bonds are formed by suitable functional groups located on polymer binder molecules. Increasing the cross-linking agent such as trimethylolpropane triacrylate (TMPTA) (Figure 2.16), concentration in the resist composition has a positive effect on the chemical stability of nanofluidic devices [61]. Therefore, the crosslinking agent concentration in the resist is an important parameter that can affect the chemical and corrosion resistance and mechanical strength of UV resin. Chemical stability also plays an important role in determining the mechanical properties of the nanofluidic devices, such as mechanical strength and surface hardness. In general, materials with higher chemical stability will be stronger and have greater hardness. Increasing the strength and hardness helps avoid an undesirable process called the swelling effect. The swelling effect is a phenomenon in which the walls of the nanodevices absorb the solution in the channels, causing the walls to swell [62]. This changes the dimensions of the nanodevice and may cause complications.

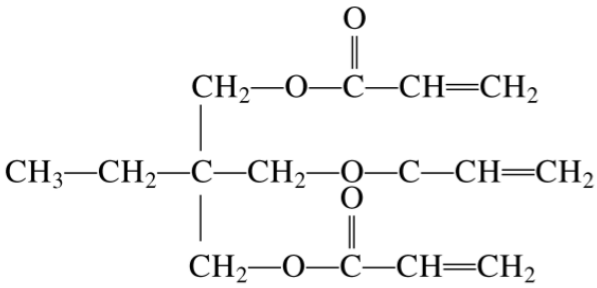

Figure 2.16. Molecule structure of trimethylolpropane triacrylate (TMPTA) [61]

In a previous experiment [59], three different polymers were used to make nanofluidic devices: COC6013, PMMA, and PEGDA. COC and PMMA are thermoplastics, meaning they are heated to their glass transition temperatures (T_g) and compressed with a hot press to create nanochannels.

PEGDA is an ultraviolet resin that can be cured by exposure to ultraviolet light. To form nanodevices, the liquid PEGDA UV resin is poured onto a PMMA backbone substrate cured with UV light. PEGDA also has the advantage of a low surface charge density; having a low surface charge density is an attractive characteristic for DNA translocation, as mentioned above. The advantages of high resolution and low surface charge density made PEGDA the best material for making these devices. The disadvantage of PEGDA is its weak chemical stability, but this can be solved with the addition of the crosslinking agent TMPTA.

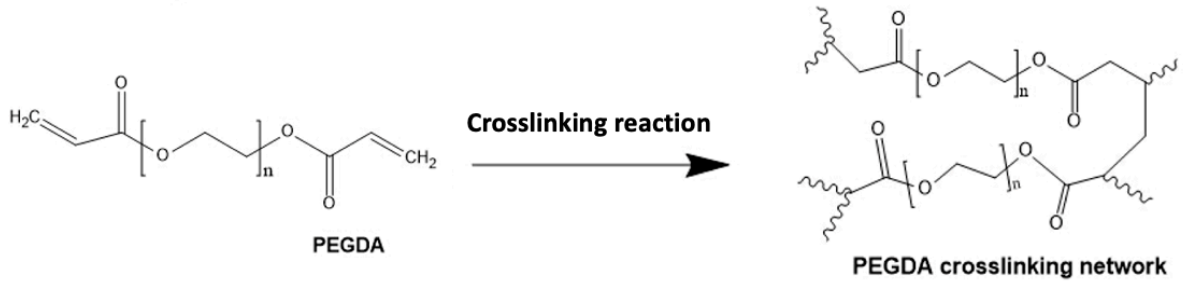

Figure 2.17. Molecule structure of crosslinked polyethlene glycol diacrylate (PEGDA) [63]

Crosslinking reactions between PEGDA and TMPTA increase the crystallinity of the PEGDA by serving as a bonding agent between PEGDA molecules (Figure 2.17). This should make the polymer more chemically stable, which was tested in this study. Higher crystallinity also implies higher mechanical strength and surface hardness; this was verified experimentally using PEGDA resin with different TMPTA concentrations. Experiments were conducted to validate the chemical and mechanical effects of TMPTA concentrations in PEGDA resins and to support the effects of TMPTA on surface charge density, DNA translocating ability, and the shrinkage of nanostructures. Adding a crosslinking agent into the PEGDA resin was shown to significantly increase its mechanical stability without significantly impacting its beneficial electrochemical properties [63].

CHAPTER 3. ZETA POTENTIAL MEASUREMENT OF POLYMERS USED FOR NANOFLUIDIC BIOSENSORS

3.1. Introduction

Nanofluidic systems are defined as systems with functional or critical dimensions of structures in the 1-100 nm range [7, 8]. In recent years, the interest in nanofluidics-based targeting single molecules has grown. This sensing technique requires at least one characteristic dimension of the confined channel below 100 nm. Three parameters in this system play significant roles in the transport of solutes and solvent passing through nanochannels or nanopores: the presence of external forces, electrokinetic forces, electrical forces between a charged wall and solute molecules, and friction forces between a wall and a solvent. Based on these forces, electrokinetic phenomena in the nanofluidic systems can be divided into four groups such as Electroosmosis, Electrophoresis, Streaming potential, and Sedimentation potential [9-12].

In the recent past, the majority of researches about nanofluidic devices have focused on using glass, fused silica or silicon (Si) as the substrate material of the devices to take their advantage such as established surface chemistry, excellent optical properties, well-established fabrication technologies, and maintainability during the thermal or pressure processing. However, these inorganic-based nanofluidic devices have critical defects such as extensive device preparation steps and high-fabrication costs. Therefore, polymers can be an attractive alternative to inorganic-based materials for nanofluidic biosensors due to their diverse range of physicochemical properties, low material cost, a variety of surface modification protocols that can be used and several fabrication techniques.

There are two general categories of polymeric materials that have been used for nanofluidic devices: (1) elastomers and (2) thermoplastics [17]. Elastomers are unstructured polymers with a few cross-links between polymer chains. While the low Young's modulus enables large deformation upon application of an external load, covalent cross-links help elastomers return

to their original shape upon release of the load. Polydimethylsiloxane, PDMS, is a good example of an elastomeric material. On the other hand, thermoplastics are usually linear or branched polymers with higher molecular weights and Young's modulus. Examples of thermoplastics are poly(methyl methacrylate), PMMA; polycarbonate, PC; and cyclo-olefincopolymer, COC.

Nanofluidic devices can be made from different polymers, such as PMMA, COC 6013, and PEGDA. These polymers have the advantages of cost-effectiveness, reproducibility, biocompatibility, and low electrical noise for electrical measurements. Polymers in a nanofluidic device have an electrokinetic surface charge density which plays a crucial role in DNA translocating. Charged surfaces will attract counter-ions in the fluid, and the counter-ions will make a wall on the charged surface. This collected counter-ion wall is called the "electric double layer" or "EDL," and it has a notable influence on the flow of electrolytes. The potential at the top layer of EDL is called the "zeta-potential," and it can be used to determine electrokinetic surface charge density. Zeta potential (ζ) and surface charge density (σ) are impactful parameters in the nanofluidic system because electrokinetic forces in the system can be straightforwardly affected by these two factors. Thus, The success of DNA translocation is determined by the electrokinetic forces near and inside nanostructure.

Tons of practical nanofabrication skills to make nanostructure on polymer-based nanofluidic devices have developed for a few decades such as photolithography, hot embossing lithography, and injection molding [52]. Nanoimprint lithography (NIL) is a practical nanolithography method which can replicate nanoscale features by mechanically pressing pre-established molds into imprint resist [53]. There are two main sub-parts of NIL. One is thermal-NIL which adjusts heat to make patterns on substrates based on the glass transition temperature (T_g) of the substrates, and the other one is ultraviolet (UV)-NIL which utilizes UV resist that

can be solidified by UV light. Despite the useful fabrication methods, the nanofluidic devices have a limitation in processes after nanostructure fabrication, such as bonding process, electrolytes filling, and long-term electrical measurement. These issues can be dealt with by modifying the surface of the material.

Extensive studies have been conducted on surface modification of the polymers for nanofluidic devices to manipulate the properties of polymers such as bonding conditions and wettability [64]. O_2 plasma is one of the most popular technique to modify the surface of polymers. O_2 plasma treatment can control surface roughness by the reaction between hydroxyl groups on the surface and O_2 molecules in the air inside the chamber. To be specific, the O_2 plasma particles impact the surface of the samples in the chamber at a high velocity due to the applied electric current between the O_2 plasma inlet and the vacuum chamber. This setup gave the O_2 molecules enough energy to create surface roughness as they interacted with the surface of the samples. Plus, the surface roughness of the inside wall of nanostructures can significantly influence the streaming current inside the nanochannels of the device, ultimately affecting the zeta potential.;Schnitzer *et al* investigated the relationship between surface roughness of the sample and zeta potential [65]. This group prepared polyester as a sample material for this experiment. They make the three different surface types such as plain, brushed, and checkered surface. The surface roughenss (R_a) of plain surface, brushed, and checkered surface is 0.09 μm, 2.24 μm, and 9.37 μm, respectively. They realized that the most rough surface which is checkered surface has the lowest zeta potentil as shown in the Figure 3.1.

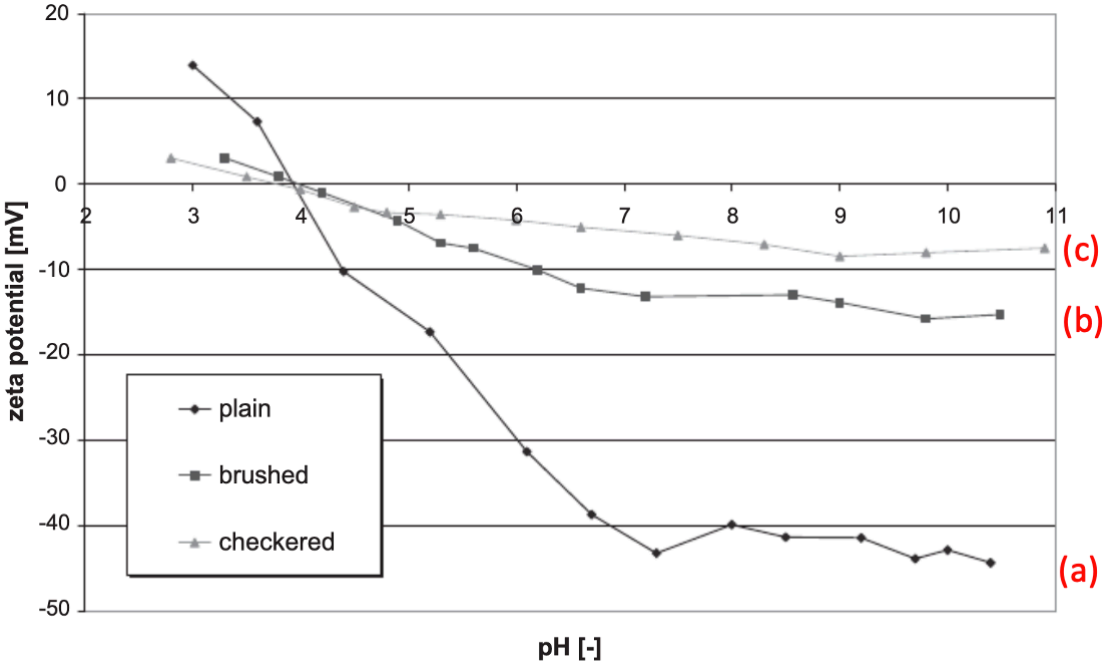

Figure 3.1. Plot of zeta potential verse pH: (a) the zeta potential of plain surface, (b) brushed surface, and (c) checkered surface.

In addition, Chai *et al.* performed O_2 plasma treatment on PMMA surfaces with differing treatment times to improve the wettability of the PMMA [66]. They carried out O_2 plasma treatment on the PMMA for periods of 1 second, 10 seconds, and 50 seconds. They found that the wettability of PMMA surfaces continued to increase over 50 seconds. They asserted that variation of the zeta potential for the plasma-treated PMMA surfaces behaves similarly to that of contact angles. Figure 3.2. shows the surface topography of untreated and plasma-treated PMMA.

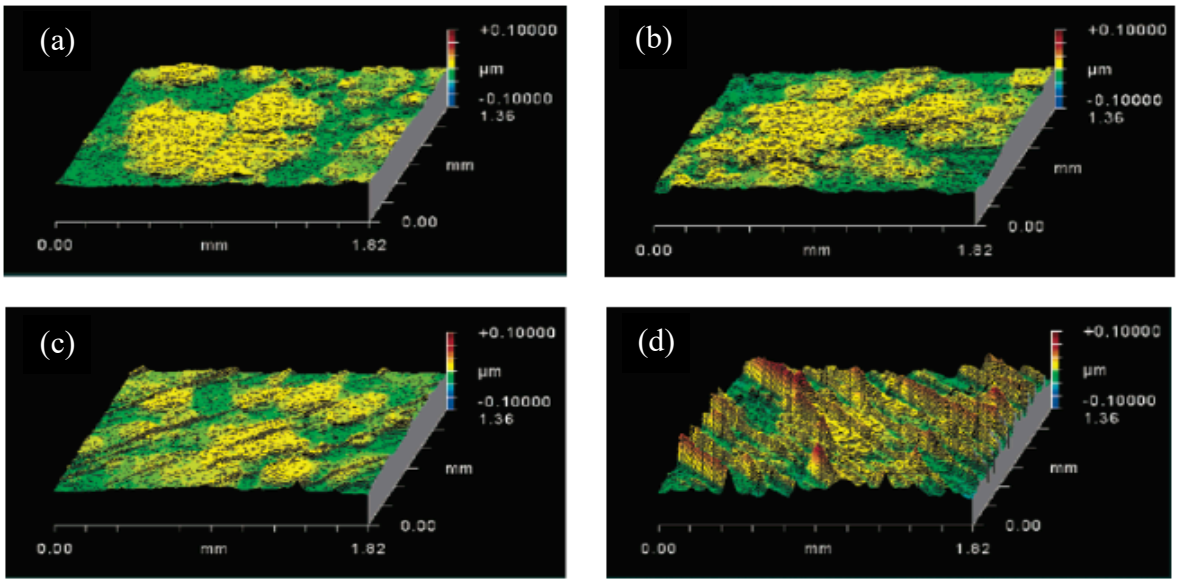

Figure 3.2. Surface topography of untreated and plasma-treated PMMA: (a) untreated PMMA, (b) O_2 plasma-treated PMMA for 1 second, (c) O_2 plasma-treated PMMA for 10 seconds, and (d) O_2 plasma-treated PMMA for 50 seconds.

O'Neil et al. explored the effect of O_2 plasma treatment on the surface properties of cyclic olefin copolymer (COC) [67]. They described how O_2 plasma is used to assist in the thermal bonding of polymer-based fluidic devices, improving the wettability of the surfaces. They studied the surface roughness variance of different cyclic concentration COC, such as COC 6013, COC 6017, and COC 8007 with different O_2 plasma treatment times. Their results showed that the RMS roughness on the COC surfaces increased as O_2 plasma time increased. Furthermore, they found that COC 8007, which has the lowest cyclic concentration, had the highest RMS roughness, which was 0.9 nm. Figure x.x shows a comparison of the AFM images of COC 8007 and COC 6017, both after O_2 plasma treatment. Figure 3.3 displays the RMS roughness versus the COC grade confirming that an increase in the norbornene mol% showed a decrease in the RMS roughness.

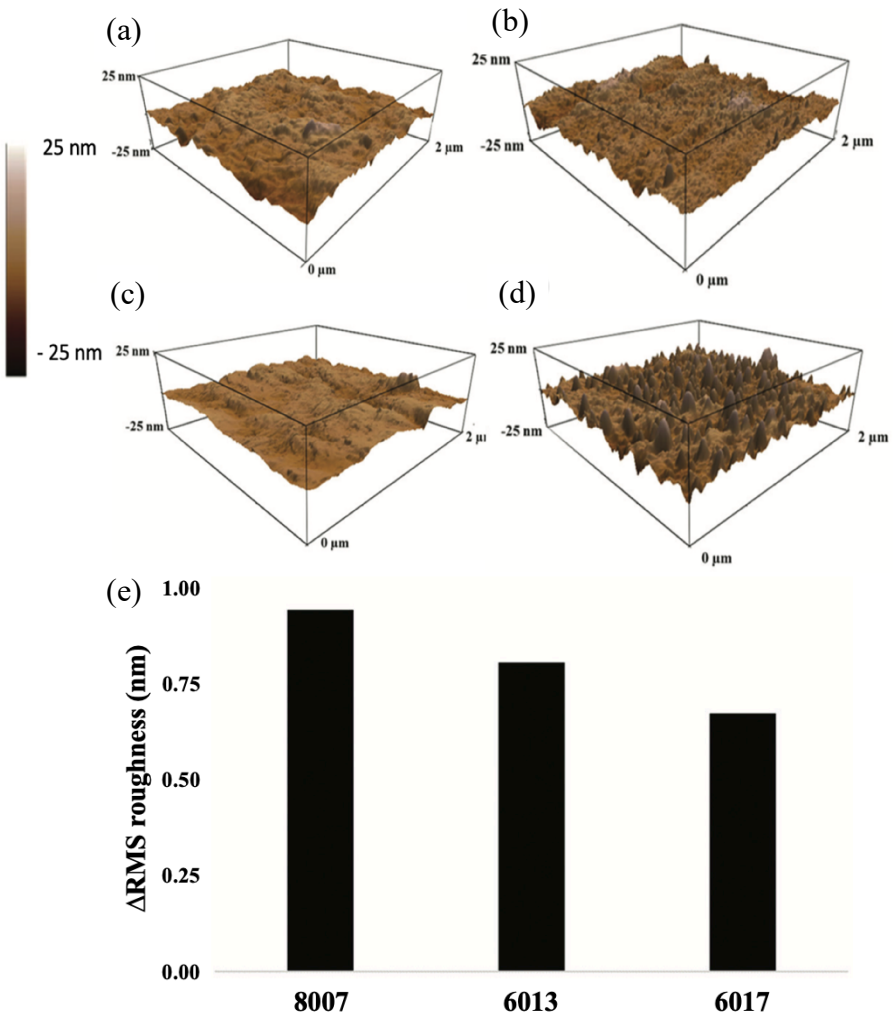

Figure 3.3. Surface topography of untreated and plasma-treated COC: (a) pristine COC 8007, (b) O_2 plasma-treated COC 8007 for 30 seconds under 50 Watt, (c) pristine COC 6017, and (d) O_2 plasma-treated COC 6017 for 30 seconds under 50 Watt. (e) The data result of the RMS roughness versus the cyclic concentration in COC [67].

In this paper, we will investigate the effects of O_2 plasma treatment on the surface roughness and furthermore on the electrokinetic surface charge density of most-used polymers for nanofluidic devices especially impact-modified PMMA, COC 6013, and PEGDA. We also define the relationship among O_2 plasma treatment, zeta potential, and electrokinetic surface charge density by measuring zeta potentials of samples O_2 treated with different treatment times according to the aging time for 3 weeks.

3.2 Experimental Method and Analysis.

3.2.1 Materials and sample preparation

We used impact-modified PMMA (ePlastics) and COC 6013 (TOPAS). PEGDA resin was made by mixing pure PEGDA (Sigma-Aldrich) with photo-initiator, Irgacure 651 (Ciba), for a ratio of 95:5. The PEGDA resin was then poured over the full surface area of a silicon substrate and covered with a 175µm impact-modified PMMA sheet (Goodfellow). The resin was cured with a UV light ($25\ mW/cm^2 at\ 365\ nm$) for 6 minutes. After UV-curing, the PEGDA samples were released from the silicon substrate. The released samples were cured with the UV light for an additional 5 minutes to be fully cured. Figure 3.4 shows the actual images of impact-modified PMMA, COC 6013, and PEGDA.

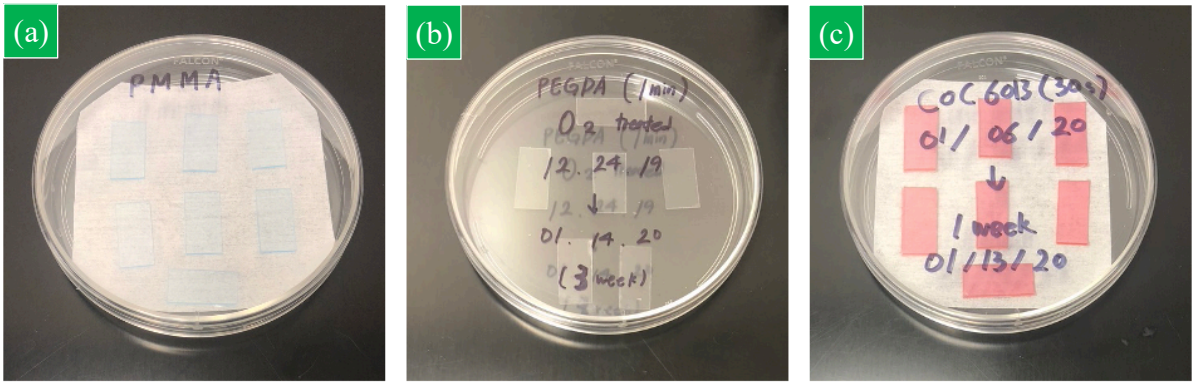

Figure 3.4. Experimental samples for zeta potential measurement (1 x 2 cm): (a) PMMA, (b) PEGDA, and (c) COC 6013

3.2.2 The principle of O_2 treatment.

O_2 treatment is the bombardment of the samples with O_2 plasma. This was conducted by placing the samples in a vacuum chamber and lowering the pressure to 150 mTorr. This pressure was maintained inside the chamber throughout the O_2 plasma activation. The electrical potential was controlled by a power source that provided 50 W of energy. The O_2 plasma particles impact the surface of the samples in the chamber at a high velocity due to the applied electric current between the O_2 plasma inlet and the vacuum chamber. This setup gave the O_2

molecules enough energy to create surface roughness as they interacted with the surface of the samples. Five types of samples were made; the first type was not treated with O_2 plasma and the remaining four types were treated for 30s, 1m, 1m 30s, and 3m, respectively.

3.2.3 zeta potential measurement by using SurPASS 3 machine and its principle

The zeta potential of each sample was measured utilizing the SurPASS 3 machine (Anton Paar) as shown in Figure 3.5 and Figure 3.6. The SurPASS 3 machine can automatically determine the zeta potential of a material's surface. This is done by feeding a flow of an aqueous electrolyte solution through the gap between two samples of material in a controlled pressure system. The SurPASS 3 measures the values of both the streaming potential and streaming current and uses them to calculate the zeta potential of the tested surface.

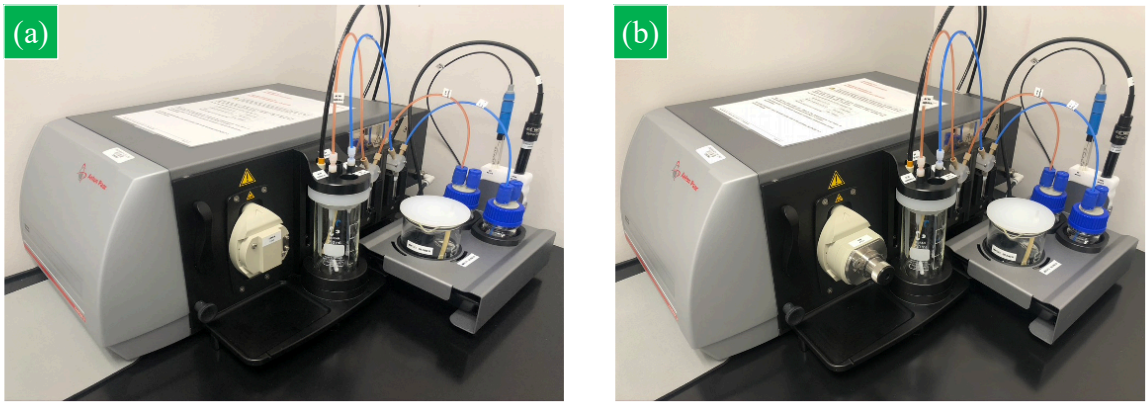

Figure 3.5. Picture of SurPASS 3 machine from Anton Paar. (a) SurPASS 3 without the adjustable gap cell and (b) SurPASS 3 machine with the adjustable gap cell.

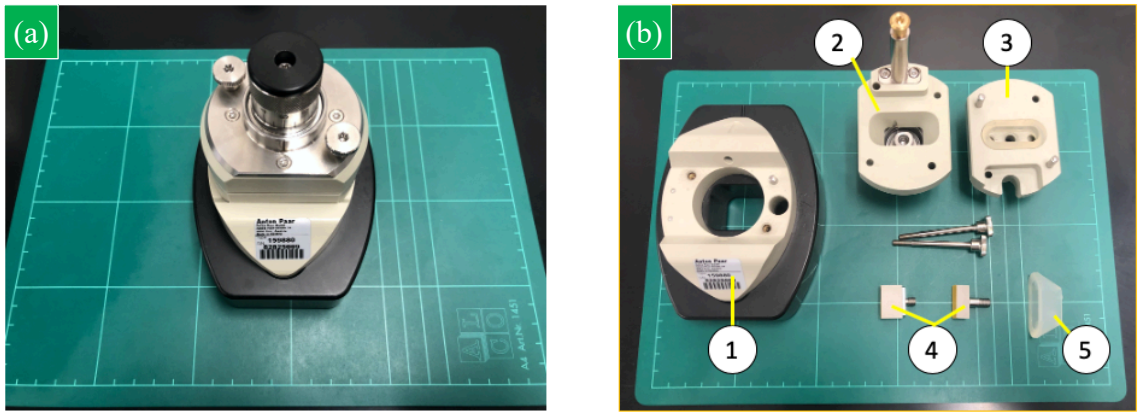

Figure 3.6. Picture of the adjustable gap cell for SurPASS 3 machine. (a) Assembled adjustable gap cell and (b) disassembled adjustable gap cell: (1) main body of the adjustable gap cell, (2) upper body of the adjustable gap cell, (3) lower body of the adjustable gap cell, (4) sample stages, and (5) gasket.

To be specific, both of the streaming potential and streaming current are measured through pressure versus time data between two sample surfaces. Two 1 cm x 2 cm samples were used for each measurement. The two samples were mounted on parallel stages shown in Figure 3.7. These stages can be adjusted to control the gap height between the two samples. The gap height was set to 100 μm for the measurement. Then, a 0.001M solution of KCl was filled into the gap. To calculate the zeta potential, the setup was pressurized to 500 mbar and gradually released to 200 mbar. The slope of the pressure versus time plot can then be used to calculate the zeta potential.

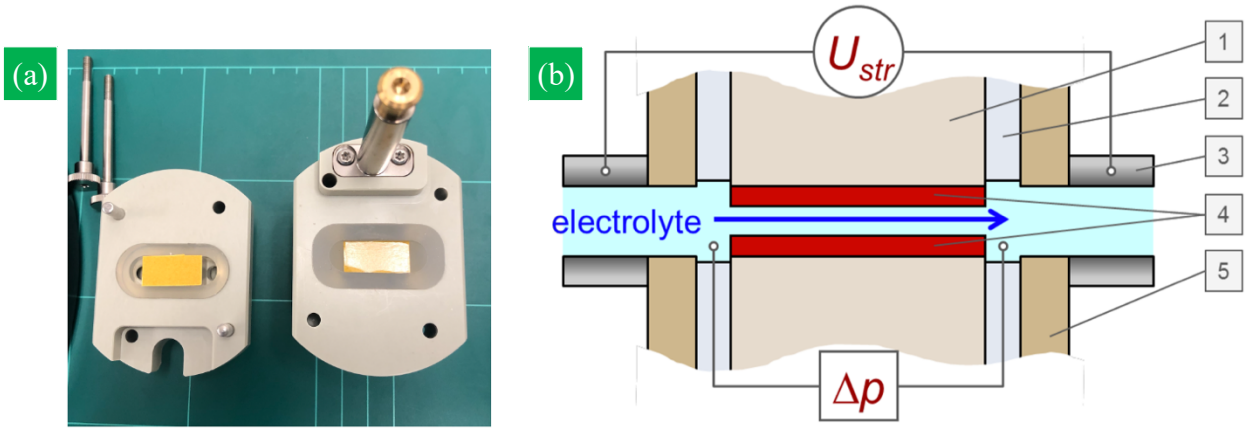

Figure 3.7. (a) Half assembled adjustable gap cell and (b) schematic figure of the adjustable gap cell: (1) sample stage, (2) gasket, (3) electrode, (4) samples, and (5) body of adjustable gap cell [68].

At least four measurements were performed at each condition. Each zeta potential value was used to calculate the average value of zeta potentials. The average value was directly converted to the electrokinetic surface charge density of the sample based on the Helmholtz-Smoluchowski equation.

3.2.4 Equation derivation

Zeta potentials for solid materials with a planar surface can be determined using the Helmholtz-Smoluchowski equation. This equation is shown below:

$$\zeta = \frac{dI_{str}}{d\Delta p} \times \frac{\eta}{\varepsilon \times \varepsilon_0} \times \frac{L}{A} \tag{3.1}$$

, where ζ is the electrokinetic potential, η is the fluid viscosity, and $\varepsilon \times \varepsilon_0$ is the dielectric coefficient of the electrolyte solution. For dilute aqueous solutions, the viscosity and dielectric coefficient of water is used. The term $dI_{str}/d\Delta p$ is related to the cell constant of the streaming channel (the gap between adjacent solid samples), L is the length of the rectangular slit channel formed between the two planar surfaces, and A is its cross-sectional area (A = W x H) with channel width W and gap height H. Figure 3.8 shows a schematic representation of the arrangement of solids with planar surfaces and indicates the key dimensions of the streaming channel.

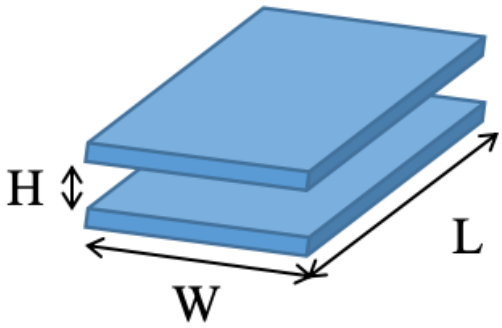

Figure 3.8. The schematic figure for the arrangement of solids with planar surfaces

The zeta potential is a phenomenological quantity closely linked to the electrokinetic surface charge density for microscale systems. This relationship can be quantified using the Grahame equation. The electrokinetic surface charge density is given by:

$$\sigma_\zeta = \frac{2\varepsilon_0 \varepsilon_r k_B T}{e\lambda_D} \sinh\left(\frac{e\zeta}{2k_B T}\right) \tag{3.2}$$

, where e is the elementary charge in (C), k_B is the Boltzmann constant in (J/K), ε_0 is the permittivity of the vacuum, ε_r is the dielectric constant of water at 20℃, F is the Faraday constant in (C/mol), T is the temperature of the room in (K), and c is the concentration of KCl in [M]. As shown, the relationship between electrokinetic surface charge density and zeta potential is defined by a non-linear function. It has also been shown that zeta potential can be used to determine the number of isoelectric points on a surface, which provides us with a method to measure changes in ionizable groups on that surface.

In the following measurements, the electrokinetic surface charge density is negative, and therefore the zeta potential is also negative. For the purpose of this paper, the zeta potential will be reported in terms of its absolute value (i.e. a “high” zeta potential is one that has a large negative value and a “low” zeta potential has a negative value relatively close to zero).

3.3. Result and discussion

3.3.1 Zeta potential of untreated impact PMMA between pH 2.5 and 10.5

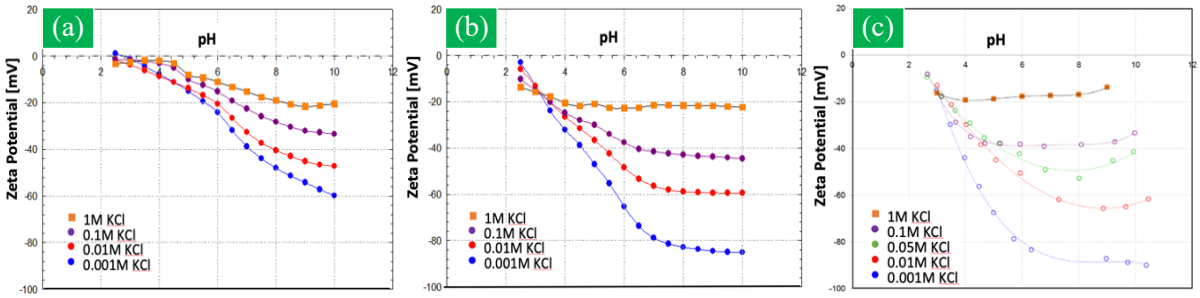

Figure 3.9. Zeta potential of PMMA substrate as a function of pH for different KCl concentrations: (a) pristine impact-modified PMMA, (b) impact-modified PMMA after O_2 plasma treatment at a power of 450 W for 30 seconds (c) impact-modified PMMA one week after O_2 plasma treatment. The measurements for Figure 3.9(c) were performed by Anton Paar. The data for 1 M KCl were obtained by extrapolating the measured zeta potential of different KCl concentrations.

Figure 3.9(a) shows the zeta potential of the impact-modified PMMA prior to O_2 plasma treatment as a function of pH for different KCl concentrations. The measurements were performed with KCl concentrations of 0.1, 0.01 and 0.001 M. The data points corresponding to the KCl concentration of 1 M were obtained by extrapolating the data points of lower concentrations with $\zeta = a + b \cdot \mathrm{p}C$, where and $\mathrm{p}C$ is defined as $-\log C$. Here, a and b are constants where C is the concentration of counterions. This linear relationship between zeta potential and $-\log C$ is known to work well for univalent electrolytes. Overall, zeta potential decreases with pH, which is attributed to an increase in the amount of de-protonation at hydrophilic sites due to low proton concentration resulting in more negative electrokinetic surface charge density. The rate of the decrease of zeta potential (i.e. the slope of zeta potential vs. pH curve) also varied with pH. At 0.001 M, the decrease of zeta potential was steeper at a pH range of 6-7, which was reduced at pH > 7 but zeta potential kept decreasing up to pH 10. At a constant pH value, zeta potential decreases with the concentration of KCl solution due to a reduction in the double-layer thickness by an increase in the ionic strength and thus effective

screening of the surface negative charges by counterions. The isoelectric point of pristine impact-modified PMMA was determined to be 2-2.5.

Figure 3.9(b) shows zeta potential of the impact-modified PMMA after O_2 plasma treatment at a power of 450 W for 30 seconds. The rate of the decrease of zeta potential, i.e. the slope of zeta potential vs. pH curve also varied with different pH. At 0.001 M, the decrease of zeta potential was steeper at a pH range of 3-7, which was reduced at pH > 7, but the zeta potential still has the trend to decrease up to pH 10. On the other hand, at a pH range of 7.5-10, the decrease in the zeta potential of impact-modified PMMA after 30 seconds O_2 plasma treatment with KCl concentrations of 1, 0.1, 0.01, and 0.001 M relatively smaller than the values at a pH range of 3-7. As figures above show, the isoelectric point (IEP) with the different KCl concentrations was extrapolated based on the data from pH 2.5 to 10, which are pH 1, pH 1.5, pH 2, and pH 2.5, respectively. The decrease in the zeta potential after O_2 plasma treatment is related to the proportional relationships between zeta potential and streaming current, and between streaming current and surface properties including wettability and roughness. It is well-known that during O_2 plasma treatment, polar functional groups containing O_2 are introduced into a surface of a polymer, causing a hydrophilic surface. Also, as the concentration of KCl solution increased, the slope of zeta potential vs. pH curve at high pH values was reduced and showed a constant value of -20 mV at 1 M KCl concentration. At a constant pH value, zeta potential also decreases with the concentration of KCl solution due to a reduction in the double-layer thickness. The behavior of zeta potential of impact-modified PMMA after 30 seconds O_2 plasma treatment is compared to the behavior of zeta potential of pristine impact-modified PMMA. After 30 seconds of O_2 plasma treatment, the zeta potential overall decreases compared to the corresponding zeta potential of pristine PMMA at all four different KCl concentrations

Figure 3.9(c) describes zeta potential of the impact-modified PMMA 1 week after O_2 plasma treatment at a power of 450 W for 30 seconds. This result indicates the equivalent trend as seen in the result with less than a 5% difference. However, zeta potential are more fluctuating 1 week after O_2 plasma treatment. It is well known that hydroxyl groups on the surface are partially recovered as the exposure time increases in the air.

3.3.2 Zeta potential and electrokinetic surface charge density with different O_2 treatment time between pH 7.5 and 10.5

Figure 3.10, 3.11, and 3.12 show zeta potential and electrokinetic surface charge density of the impact-modified PMMA, COC 6013, and PEGDA with different O_2 plasma treatment times as a function of pH at 0.001M KCl concentrations with 3 weeks aging time period. These figures preponderantly explicate the difference of zeta potentials among impact-modified PMMA, COC 6013, and PEGDA at a pH range of 7.5-10. The surfaces of samples are treated with O_2 plasma at a power of 450 W for 30 seconds, 1 minute, 1 minute 30 seconds, and 3 minutes. This linear relationship between zeta potential and -log C is known to work well for univalent electrolytes. Before the O_2 plasma treatment, zeta potential decreases with increasing pH, which is attributed to an increase in the amount of de-protonation at hydrophilic sites due to low proton concentration resulting in more negative electrokinetic surface charge density.

PMMA initially had a zeta potential of -51.6 ± 3.04 mV and an electrokinetic surface charge density of -4.7 ± 0.40 mC/m^2. For samples treated for 30 seconds; the zeta potentials right after, one week after, and three weeks after treatment were -79.0 ± 4.41 mV, -92.6 ± 1.25 mV, and -93.3 ± 1.96 mV, respectively. The surface charge densities of those samples at the same time intervals were -9.3 ± 0.98 mC/m^2, -12.6 ± 0.33 mC/m^2, and -12.8 ± 0.53 mC/m^2. For samples treated for three minutes; the zeta potentials right after, one week after, and three weeks after treatment were -51.3 ± 2.25 mV, -49.8 ± 4.68 mV, and -52.3 ± 2.89 mV,

respectively. The surface charge densities at the same time intervals were -4.7 ± 0.33 mC/m^2, -4.5 ± 0.65 mC/m^2, and -4.8 ± 0.43 mC/m^2.

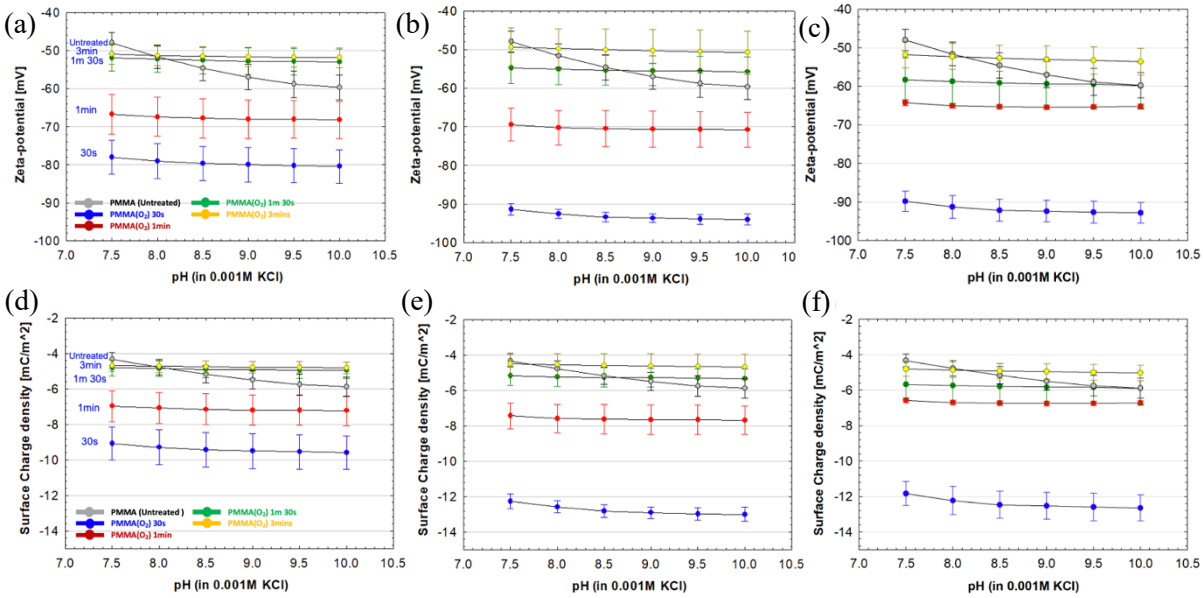

Figure 3.10. Plots of zeta potential and electrokinetic surface charge density of O_2 treated PMMA with aging time: (a) zeta potential right after O_2 plasma treatment, (b) zeta potential 1 week after O_2 plasma, (c) zeta potential 3 weeks after O_2 plasma, (d) electrokinetic surface charge density right after O_2 plasma, (e) electrokinetic surface charge density 1 week after O_2 plasma, and (f) electrokinetic surface charge density 3 weeks after O_2 plasma.

Table 3.1. Zeta potential and electrokinetic surface charge density at pH 8.0 of O_2 plasma-treated PMMA according to the aging time.

PMMA		Right After	1 Week	3 Weeks
Untreated	ζ [mV]	-51.6 ± 3.05	-	-
	σ [mC/m2]	-4.8 ± 0.40	-	-
30s	ζ [mV]	-79.0 ± 4.41	-92.6 ± 1.25	-93.3 ± 1.96
	σ [mC/m2]	-9.3 ± 0.98	-12.6 ± 0.33	-12.8 ± 0.53
1m	ζ [mV]	-67.4 ± 3.87	-70.5 ± 4.19	-65.0 ± 0.62
	σ [mC/m2]	-7.1 ± 0.87	-7.6 ± 0.80	-6.7 ± 0.12
1m 30s	ζ [mV]	-52.3 ± 2.95	-55.1 ± 3.29	-58.7 ± 4.87
	σ [mC/m2]	-4.9 ± 0.45	-5.2 ± 0.53	-5.7 ± 0.91

	ζ [mV]	-51.3 ± 2.25	-49.8 ± 4.68	-52.3 ± 2.89
3m	σ [mC/m2]	-4.7 ± 0.33	-4.5 ± 0.65	-4.8 ± 0.43

COC 6013 initially had a zeta potential of -56.7 ± 7.75 mV and an electrokinetic surface charge density of -5.4 ± 1.15 mC/m^2. For samples treated for thirty seconds; the zeta potentials right after, one week after, and three weeks after treatment were -63.1 ± 9.08 mV, -42.2 ± 12.87 mV, and -45.1 ± 8.96 mV, respectively. The surface charge densities of those samples at the same time intervals were -6.4 ± 1.69 mC/m^2, -3.7 ± 1.75 mC/m^2, and -4.0 ± 1.17 mC/m^2. For samples treated for three minutes; the zeta potentials right after, one week after, and three weeks after treatment were -36.2 ± 5.07 mV, -45.1 ± 8.96 mV, and -40.3 ± 3.52 mV, respectively. The surface charge densities at the same time intervals were -3.0 ± 0.57 mC/m^2, -3.6 ± 1.25 mC/m^2, and -3.5 ± 0.37 mC/m^2.

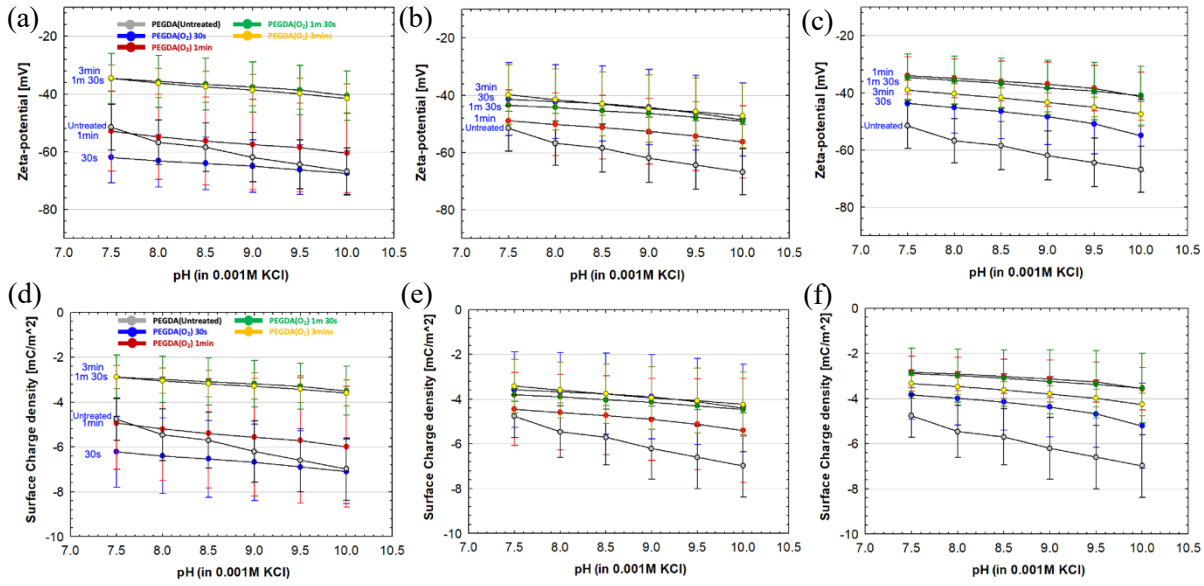

Figure 3.11. Plots of zeta potential and electrokinetic surface charge density of O_2 treated COC 6013 with aging time: (a) zeta potential right after O_2 plasma treatment, (b) zeta potential 1 week after O_2 plasma, (c) zeta potential 3 weeks after O_2 plasma, (d) electrokinetic surface charge density right after O_2 plasma, (e) electrokinetic surface charge density 1 week after O_2 plasma, and (f) electrokinetic surface charge density 3 weeks after O_2 plasma.

Table 3.2. Zeta potential and electrokinetic surface charge density at pH 8.0 of O_2 plasma-treated COC 6013 according to the aging time.

COC 6013		Right After	1 Week	3 Weeks
Untreated	ζ [mV]	-56.8 ± 7.75	-	-
	σ [mC/m2]	-5.4 ± 1.15	-	-
30s	ζ [mV]	-63.1 ± 9.08	-42.2 ± 12.87	-45.1 ± 8.96
	σ [mC/m2]	-6.4 ± 1.69	-3.7 ± 1.75	-4.0 ± 1.17
1m	ζ [mV]	-54.8 ±1 4.77	-50.1 ± 10.95	-34.9 ± 6.76
	σ [mC/m2]	-5.2 ± 2.31	-4.6 ± 1.69	-2.9 ± 0.73
1m 30s	ζ [mV]	-35.6 ± 9.00	-44.2 ± 2.14	-35.6 ± 8.49
	σ [mC/m2]	-3.0 ± 1.03	-3.9 ± 0.28	-3.0 ± 1.17
3m	ζ [mV]	-36.2 ± 5.07	-45.1 ± 8.96	-40.3 ± 3.52
	σ [mC/m2]	-3.0 ± 0.57	-3.6 ± 1.25	-3.5 ± 0.37

PEGDA initially had a zeta potential of -70.8 ± 2.73 mV and an electrokinetic surface charge density of -7.6 ± 0.54 mC/m^2. For samples treated for thirty seconds; the zeta potentials right after, one week after, and three weeks after treatment were -86.2 ± 5.96 mV, -82.1 ± 1.18 mV, and -73.4 ± 4.65 mV, respectively. The surface charge densities of those samples at the same time intervals were -10.9 ± 1.74 mC/m^2, -9.97 ± 0.28 mC/m^2, and -8.1 ± 0.88 mC/m^2. For samples treated for three minutes; the zeta potentials right after, one week after, and three weeks after treatment were -64.6 ± 2.71 mV, -62.3 ± 1.84 mV, and -66.7 ± 3.60 mV, respectively. The electrokinetic surface charge densities at the same time intervals were -6.6 ± 0.57 mC/m^2, -6.3 ± 0.32 mC/m^2, and -7.0 ± 0.73 mC/m^2.

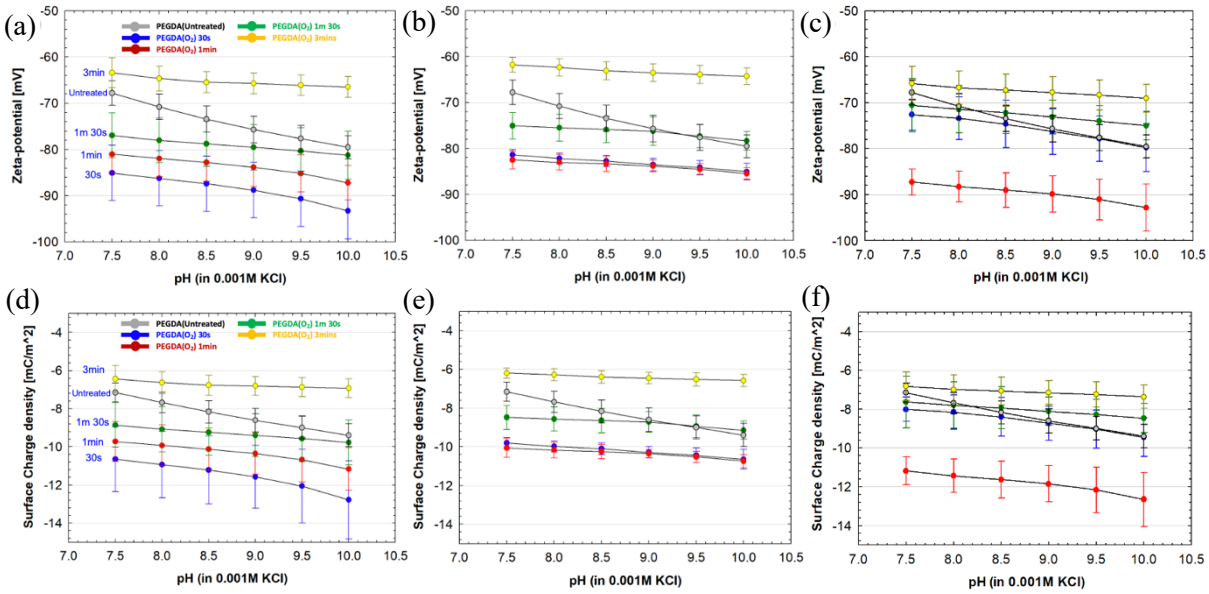

Figure 3.12. Plots of zeta potential and electrokinetic surface charge density of O_2 treated PEGDA with aging time: (a) zeta potential right after O_2 plasma treatment, (b) zeta potential 1 week after O_2 plasma, (c) zeta potential 3 weeks after O_2 plasma, (d) electrokinetic surface charge density right after O_2 plasma, (e) electrokinetic surface charge density 1 week after O_2 plasma, and (f) electrokinetic surface charge density 3 weeks after O_2 plasma.

Table 3.3. Zeta potential and electrokinetic surface charge density at pH 8.0 of O_2 plasma-treated PEGDA according to the aging time.

PEGDA		Right After	1 Week	3 Weeks
	ζ [mV]	-70.8 ± 2.73	-	-
Untreated	σ [mC/m2]	-7.7 ± 0.54	-	-
	ζ [mV]	-86.2 ± 5.96	-82.1 ± 1.18	-73.4 ± 4.65
30s	σ [mC/m2]	-10.9 ± 1.74	-9.97 ± 0.28	-8.1 ± 0.88
	ζ [mV]	-81.9 ± 3.97	-83.0 ± 1.7	-88.3 ± 3.37
1m	σ [mC/m2]	-9.9 ± 1.07	-10.2 ± 0.41	-11.4 ± 0.85
	ζ [mV]	-78.0 ± 4.88	-75.5 ± 2.89	-71.4 ± 5.13
1m 30s	σ [mC/m2]	-9.1 ± 1.18	-8.6 ± 0.63	-7.8 ± 1.20
	ζ [mV]	-64.6 ± 2.71	-62.3 ± 1.84	-66.7 ± 3.60
3m	σ [mC/m2]	-6.6 ± 0.57	-6.3 ± 0.32	-7.0 ± 0.73

After the 30 seconds of O_2 plasma treatment, the decrease in zeta potential with increasing pH is reduced compared to the zeta potential of untreated samples. The decrease in the zeta potential after O_2 plasma treatment is related to the proportional relationships between zeta potential and streaming current, essentially due to the relationship between streaming current and surface properties including wettability and roughness. It is well-known that during O_2 plasma treatment, polar functional groups containing O_2 are introduced into a surface of a polymer, causing a hydrophilic surface [66]. Furthermore, with over 30 seconds O_2 plasma treatment, the effect of surface roughness on the zeta potential is more significant than its of wettability. In this case, surface roughness becomes rougher after O_2 plasma treatment up to the point at which the roughness no longer be changed by O_2 plasma treatment. To be specific, the rougher surface will decrease the electro-osmosis flow due to the friction between the sample surface and electrolytes, reducing the streaming current [65]. Then, the decreasing streaming current proportionally affects the zeta potential based on the relationship between the streaming current and the zeta potential in the Helmholtz-Smoluchowski equation. This is the reason why the zeta potential is changed after O_2 plasma. We will indicate the effect of the again time after O_2 plasma on the zeta potential at pH 8.0 of polymers including impact-modified PMMA, COC 6013, and PEGDA in the next chapter.

3.3.3 Comparison to Zeta potential and electrokinetic surface charge density measurement with different O_2 treatment time at pH 8.0

We point out the effect of the aging time after O_2 plasma treatment on the surface of polymers on the electrokinetic surface charge density by measuring the zeta potential values. Figure 3.13, Figure 3.15, and Figure 3.17 show the zeta potential of the impact-modified PMMA, COC 6013, PEGDA with different O_2 plasma treatment times as a function of O_2 treatment time at pH 8.0 and 0.001M KCl concentrations according to three different aging periods. Figure 3.14, Figure 3.16, and Figure 3.18 show the electrokinetic surface charge density of the impact-modified PMMA, COC 6013, PEGDA with different O_2 plasma treatment times as a function of O_2 treatment time at pH 8.0 and 0.001M KCl concentrations according to three different aging periods. Before the O_2 plasma treatment, zeta potential decreases with increasing pH, which is attributed to an increase in the amount of de-protonation at hydrophilic sites due to low proton concentration resulting in more negative electrokinetic surface charge density. The wettability improvements of PMMA, COC 6013, and PEGDA by O_2 plasma treatment are caused by the increase in surface free energy. The increase of the surface energy of polymers by O_2 plasma treatment is related to the formation of polar bonds at the surface. The reaction of these polar bonds occurs during the aging in the air. To be specific, positive ions from the O_2 plasma react and neutralize at the partially negatively charged carbonyl O_2. After that, the created electron-hole in the carbonyl group becomes filled by an electron transfer from the non-polar C-C bond, cleaving side chains from the polymer backbone. The reaction between polar bonds on the surfaces of polymers affect the zeta potential changes during the aging. The amount of the reactions causes the different trends of zeta potential of each polymer. The results are shown in the figures below.

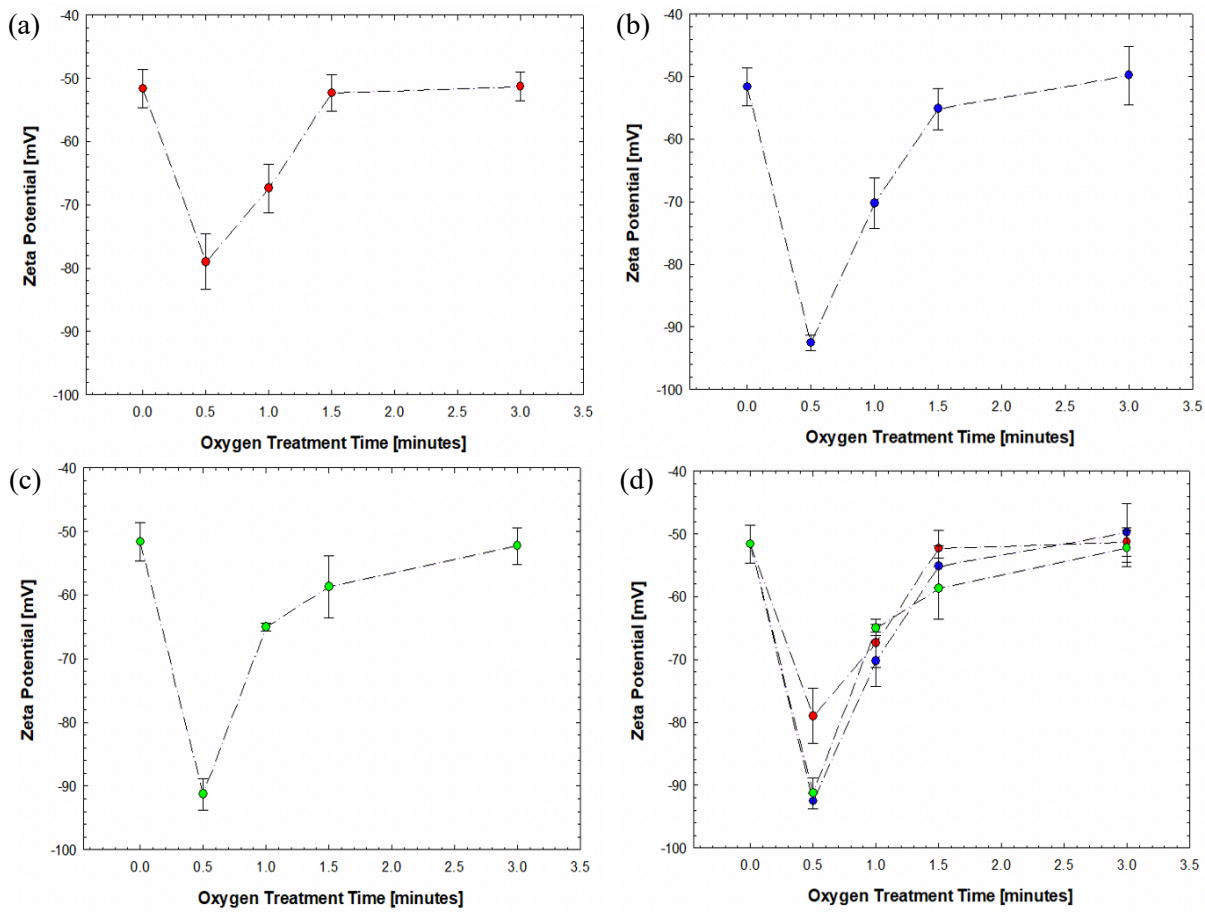

Figure 3.13. Plots of Zeta Potentials of PMMA with different O_2 treatment time at pH 8.0: (a) zeta potential right after O_2 plasma treatment, (b) zeta potential 1 week after O_2 plasma, (c) zeta potential 3 weeks after O_2 plasma, (d) combined plot of zeta potential of all three conditions.

The absolute value of the zeta potential measured right after O_2 treatment initially increased by 27 mV after 30 seconds of O_2 treatment. The absolute value of zeta potential tends to decrease from 30 seconds of O_2 treatment to 3 minutes of O_2 treatment with all aging time conditions. The decrease in the absolute value of zeta potential from 1 minute and 30 seconds of O_2 treatment to 3 minutes is relatively insignificant compared to the large gap observed from 30 seconds to 1 minute and 30 seconds with all aging time conditions.

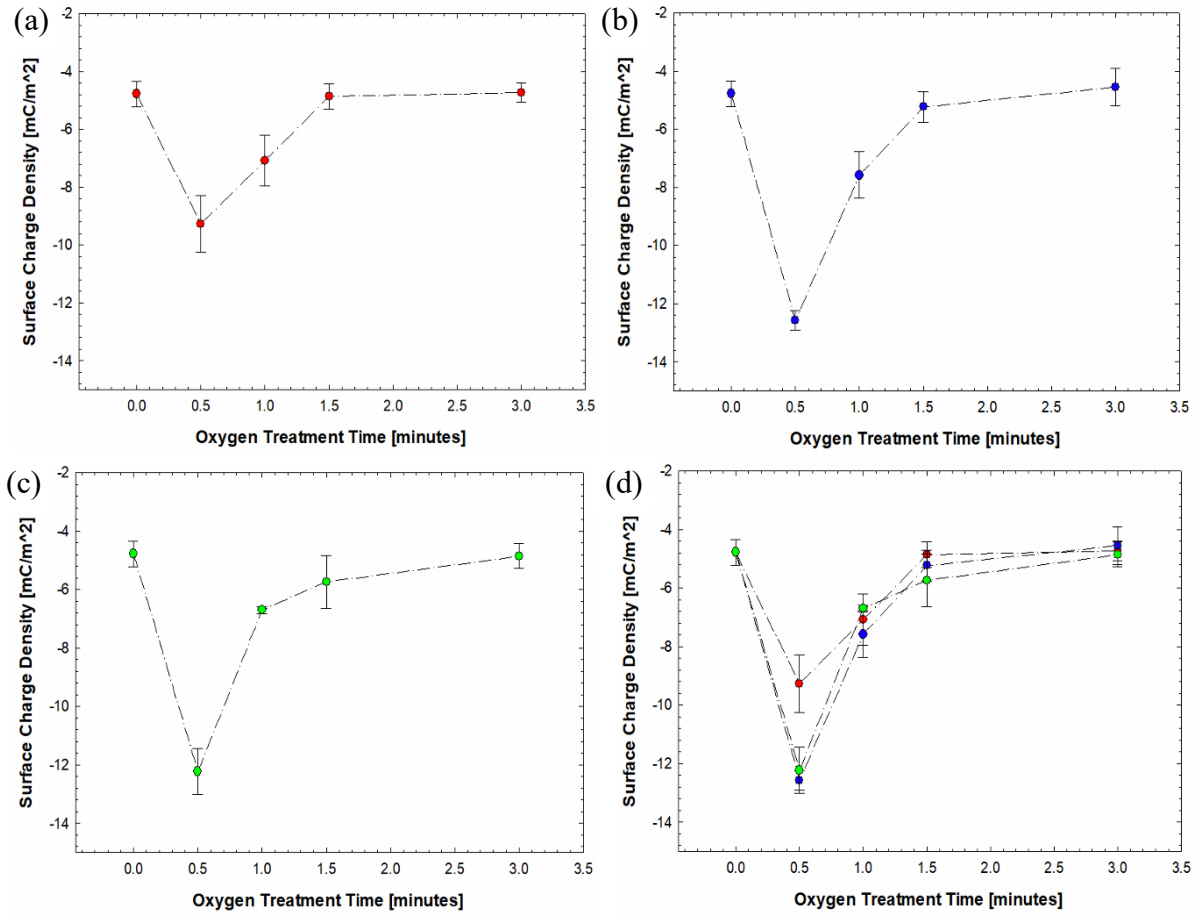

Figure 3.14. Plots of electrokinetic surface charge density of PMMA with different O_2 treatment time at pH 8.0: (a) electrokinetic surface charge density right after O_2 plasma treatment, (b) electrokinetic surface charge density 1 week after O_2 plasma, (c) electrokinetic surface charge density 3 weeks after O_2 plasma, (d) combined plot of electrokinetic surface charge density of all three conditions.

The absolute value of electrokinetic surface charge density measured right after O_2 treatment initially increased by 4.6 mC/m^2 after 30 seconds of O_2 treatment. The absolute value of electrokinetic surface charge density tends to decrease from 30 seconds of O_2 treatment to 3 minutes of O_2 treatment with all aging time conditions. The decrease in the absolute value of electrokinetic surface charge density from 1 minute and 30 seconds of O_2 treatment to 3 minutes is relatively insignificant compared to the large decrease observed from 30 seconds to 1 minute and 30 seconds with all aging time conditions.

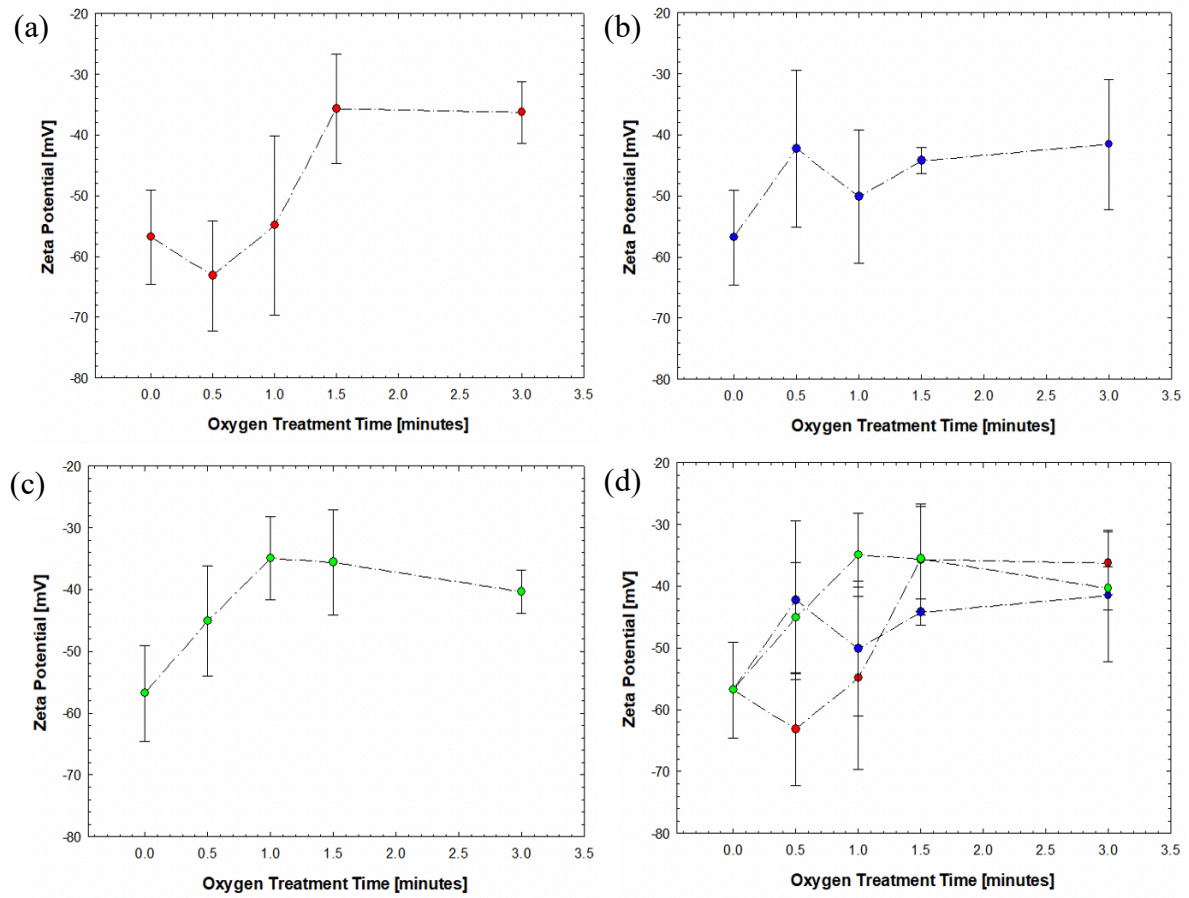

Figure 3.15. Plots of Zeta Potentials of COC 6013 with different O_2 treatment time at pH 8.0: (a) zeta potential right after O_2 plasma treatment, (b) zeta potential 1 week after O_2 plasma, (c) zeta potential 3 weeks after O_2 plasma, (d) combined plot of zeta potential of all three conditions.

There is no large decrease in the absolute value of zeta potential from the untreated value. For all aging time conditions, the absolute value of zeta potential tends to decrease as O_2 treatment time increases. It is assumed that this is due to changes in the surface roughness. With respect to the increase in the aging time, the observed range in the zeta potential decreases as the O_2 treatment time increases.

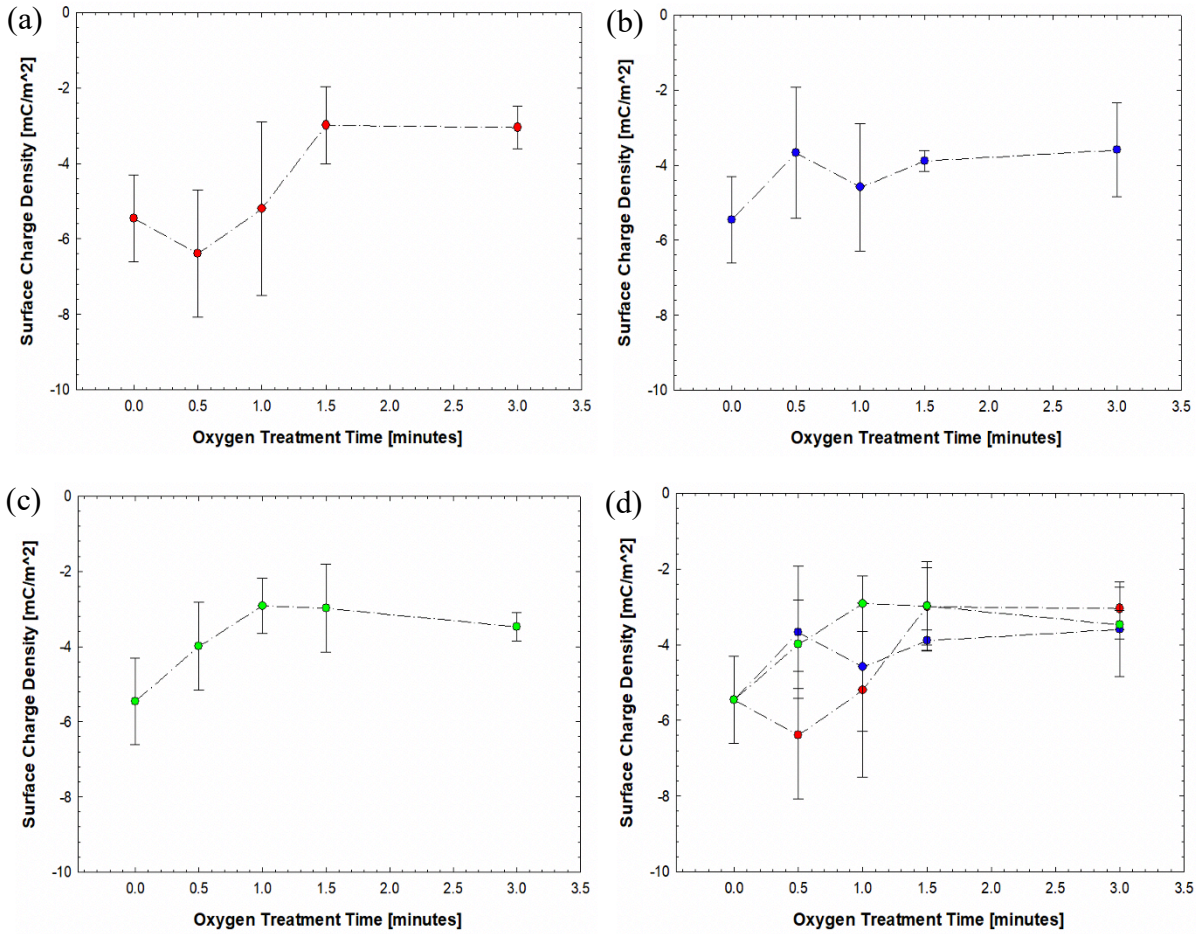

Figure 3.16. Plots of electrokinetic surface charge density of COC 6013 with different O_2 treatment time at pH 8.0: (a) electrokinetic surface charge density right after O_2 plasma treatment, (b) electrokinetic surface charge density 1 week after O_2 plasma, (c) electrokinetic surface charge density 3 weeks after O_2 plasma, (d) combined plot of electrokinetic surface charge density of all three conditions.

There is no large decrease in the absolute value of electrokinetic surface charge density from the untreated value. For all aging time conditions, the absolute value of electrokinetic surface charge density tends to decrease as O_2 treatment time increases. It is assumed that this is due to changes in the surface roughness. With respect to the increase in the aging time, the observed range in the electrokinetic surface charge density decreases as the O_2 treatment time increases.

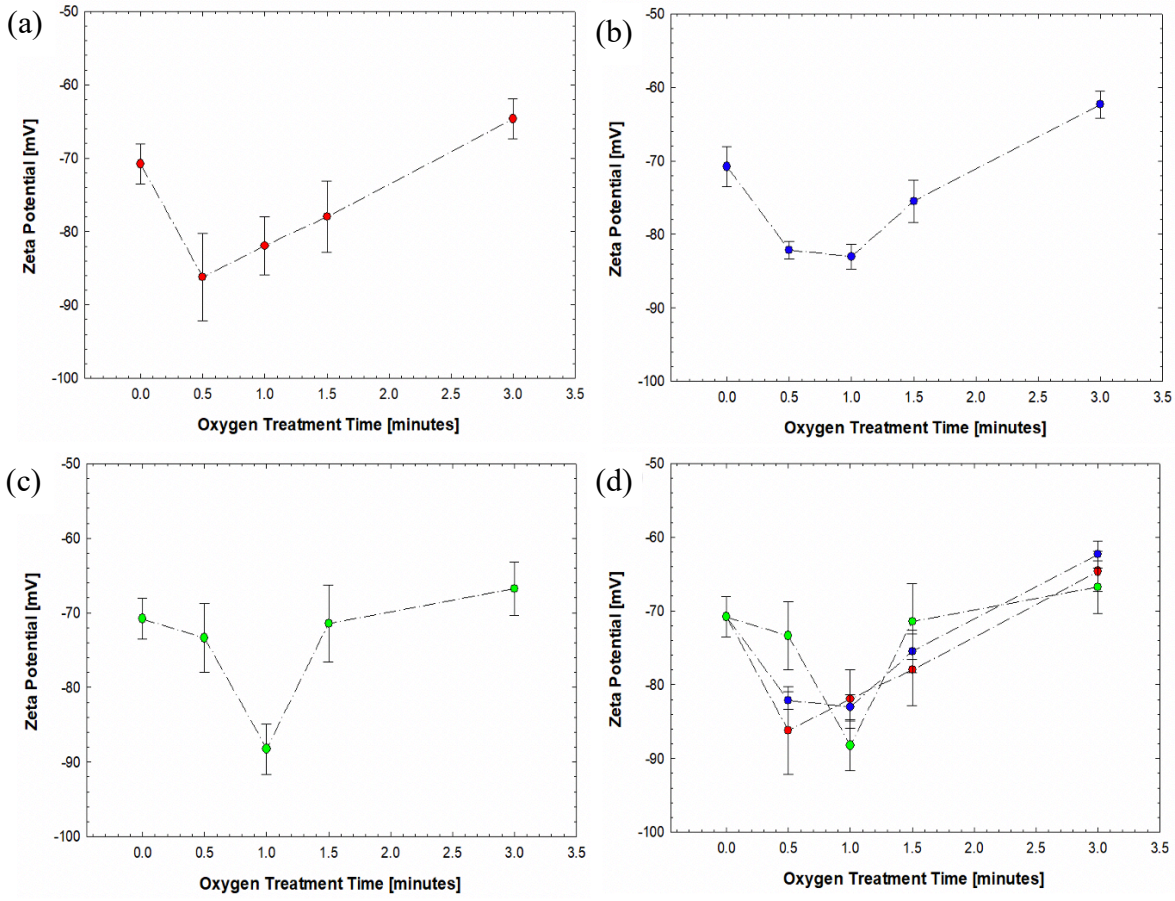

Figure 3.17. Plots of Zeta Potentials of PEGDA with different O_2 treatment time at pH 8.0: (a) zeta potential right after O_2 plasma treatment, (b) zeta potential 1 week after O_2 plasma, (c) zeta potential 3 weeks after O_2 plasma, (d) combined plot of zeta potential of all three conditions.

There is a significant decrease in the absolute value of zeta potential from the untreated value. To be specific, the zeta potential of 30 seconds O_2 treated samples tend to come back to the untreated zeta potential values as the aging time increases. The zeta potential values of samples treated for more than 1 minute do not return to the zeta potential value of untreated samples even as the aging time increases.

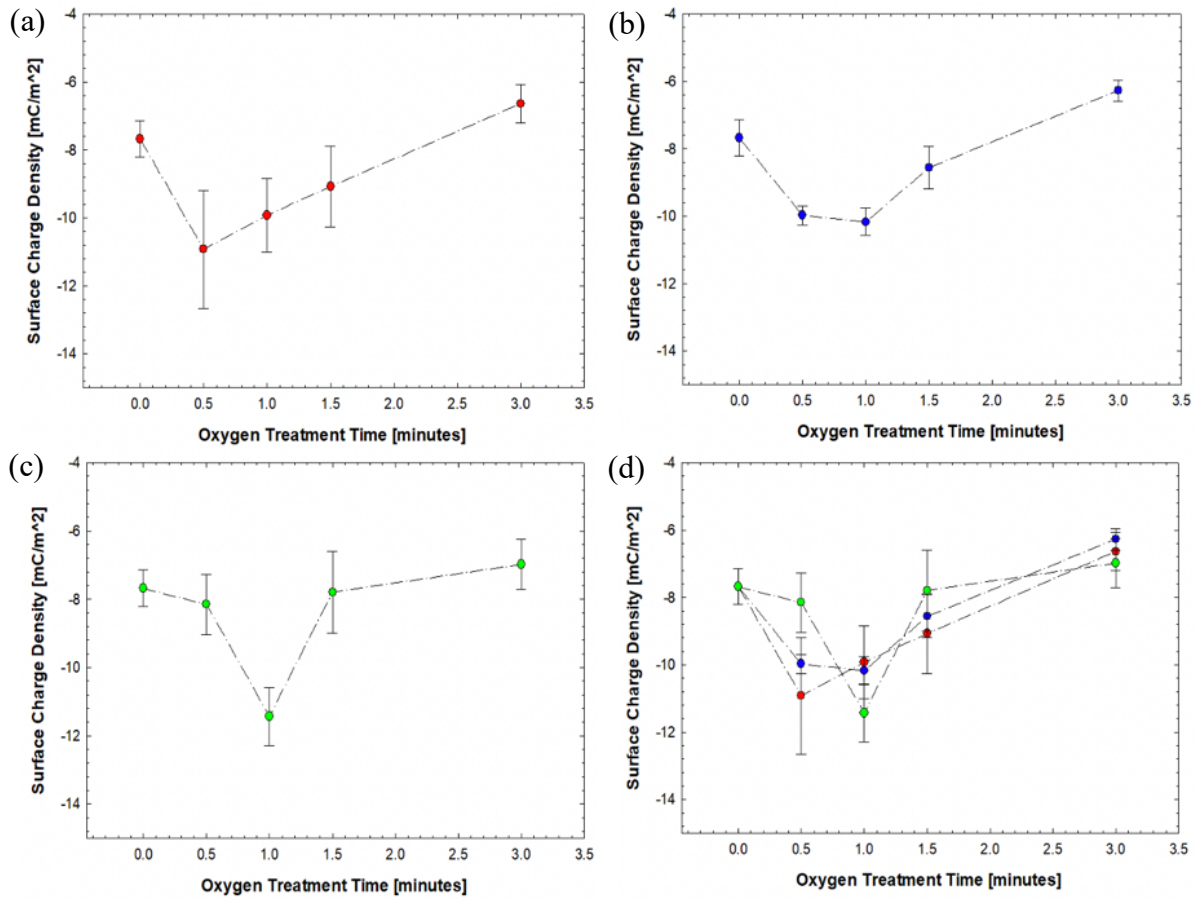

Figure 3.18. Plots of electrokinetic surface charge density of PEGDA with different O_2 treatment time at pH 8.0: (A) electrokinetic surface charge density right after O_2 plasma treatment, (B) electrokinetic surface charge density 1 week after O_2 plasma, (C) electrokinetic surface charge density 3 weeks after O_2 plasma, (D) combined plot of electrokinetic surface charge density of all three conditions.

There is a significant decrease in the absolute value of electrokinetic surface charge density from the untreated value. To be specific, the electrokinetic surface charge density of 30 seconds O_2 treated samples tend to come back to the untreated electrokinetic surface charge density values as the aging time increases. The electrokinetic surface charge density values of samples treated for more than 1 minute do not return to the electrokinetic surface charge density value of untreated samples even as the aging time increases.

The zeta-potential of PEGDA O_2 treated for 30 seconds shows a tendency to return to its untreated zeta potential value at a relatively faster rate than the other polymers during the three weeks aging time as shown in Figure 3.19. The slope of the zeta-potential and electrokinetic surface charge density curves decreased as O_2 treatment time increased. The electrokinetic surface charge density of PEGDA without O_2 treatment at pH 8.0 was -7.7 mC/m^2. The electrokinetic surface charge density of PEGDA samples O_2 treated for thirty seconds decreased more than those of the other polymers when measured for three weeks. The zeta potential of COC 6013 without O_2 treatment at pH 8.0 was -56.8 mV and the untreated electrokinetic surface charge density at pH 8.0 was -5.5 mC/m^2. The zeta potentials and electrokinetic surface charge densities of the COC 6013 samples at three weeks fluctuated more than those of PMMA and PEGDA. As we mentioned above, the reaction between polar bonds on the surfaces of polymers is closely related to the zeta potential changes during the aging, leading to the different trends of zeta potential of each polymer according to the amount and velocity of the reaction on the sample surfaces.

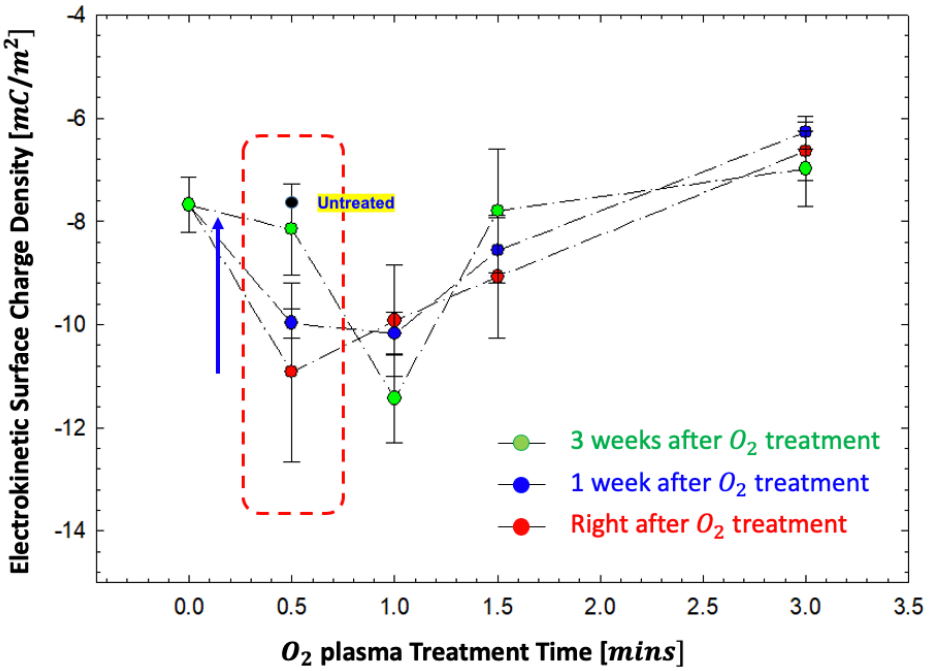

Figure 3.19. Zeta potential variation of 30 seconds O_2 plasma-treated PEGDA with 3 weeks aging time.

3.3.4 Converted electrokinetic surface charge density from the zeta potential of untreated impact-modified PMMA, COC 6013, PETG, PEGDA, COC 7010, and COC 8007

We defined the electrokinetic surface charge density of most-used polymers for nanofluidic biosensors including impact-modified PMMA, COC 6013, PETG, PEGDA, COC 7010, and COC 8007 by measuring and converting the zeta potentials of these polymers based on Equation 3.2 (Figure 3.20). It should be mentioned that the measurements were performed with KCl concentrations of 0.001 M. within the pH range of 7.5 – 10. All polymer samples are untreated. Overall, electrokinetic surface charge density decreases with increasing pH. More negative electrokinetic surface charge density is caused by an increase in the amount of de-protonation at hydrophilic sites due to low proton concentration.

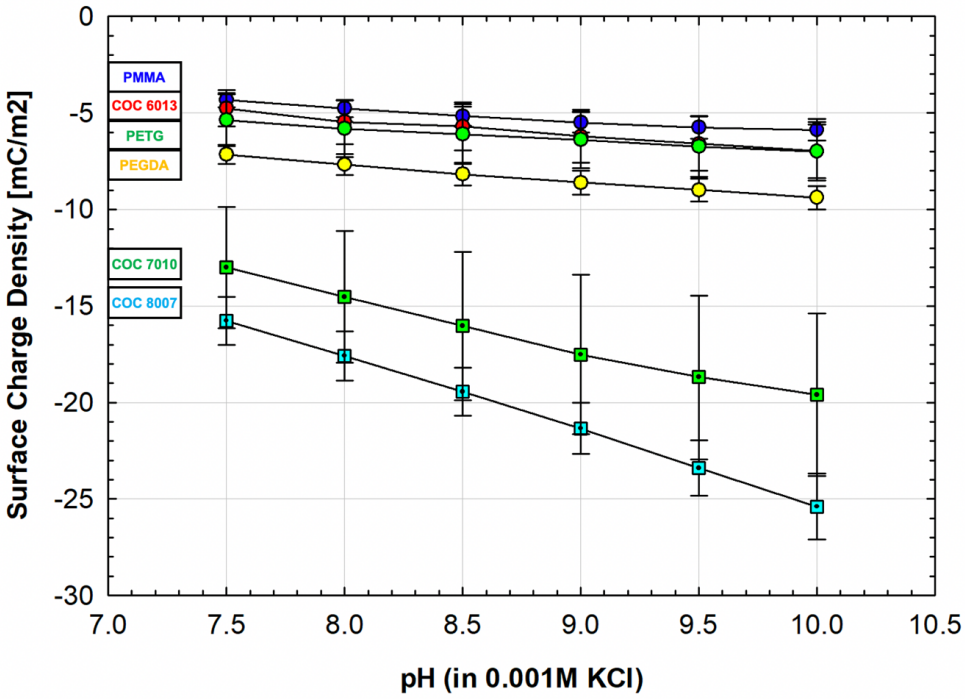

Figure 3.20. the electrokinetic surface charge density of untreated impact-modified PMMA, COC 6013, PETG, PEGDA, COC 7010, and COC 8007.

Table 3.4. Zeta potential and electrokinetic surface charge density of untreated impact-modified PMMA, COC 6013, PETG, PEGDA, COC 7010, and COC 8007.

	Zeta Potential (mV)	Electrokinetic surface charge density (mC/m^2)
IM-PMMA	- 51.6 $\pm$ 3.05	-4.8 $\pm$ 0.40
COC 6013	-56.8 $\pm$ 7.75	-5.5 $\pm$ 1.15
PETG	-59.3 $\pm$ 8.44	-5.8 $\pm$ 1.48
PEGDA	- 70.8 $\pm$ 2.73	-7.7 $\pm$ 0.54
COC 7010	-99.1 $\pm$ 10.08	-14.5 $\pm$ 3.42
COC 8007	-107.9 $\pm$ 2.70	-17.6 $\pm$ 1.27

All electrokinetic surface charge density of untreated impact-modified PMMA, COC 6013, PETG, PEGDA, COC 7010, and COC 8007 from pH 7.5 to pH 10. The impact-modified PMMA shows the lowest absolute value of electrokinetic surface charge density, which is $-4.8\ mC/m^2$ and the COC 8007 has the highest value which is $-17.6\ mC/m^2$. In particular, there are huge gaps in electrokinetic surface charge density values among the COC polymer group. The only difference of the COC group is cyclic concentration. Based on this result, we can assume that electrokinetic surface charge density can be changed and further controlled by adding other molecules such as additives or crosslinking agents. Therefore, we add a crosslinking agent into the PEGDA to explore the effect of a crosslinking agent on the electrokinetic surface charge density. We will show the results and details in the next chapter.

3.4. Conclusion

We investigated zeta potential and electrokinetic surface charge density of impact-modified PMMA, COC 6013, and PEGDA under different O_2 plasma treatment conditions (0 – 3mins treatment time and 3 weeks aging time). By material selections, we can manipulate the zeta potential and electrokinetic surface charge density of plastic devices. The variations of zeta potential or electrokinetic surface charge density upon O_2 plasma treatment is determined by the interplay between surface functionalization and surface roughness. Based on this study, we can determine the optimal O_2 plasma treatment conditions which lead to the lowest electrokinetic surface charge density for each polymer.

CHAPTER 4. EFFECT OF CROSSLINKING AGENT (TMPTA) ON PEGDA UV-RESIN

4.1. Introduction

Nanofluidic systems are defined as systems with functional dimensions of structures in the 1-100 nm range [7, 8]. The interest in the nanofluidics devices used for sensing biomolecules such as DNA has been grown in the recent years. There are four main phenomena in nanofluidic devices such as electroosmosis, electrophoresis, streaming potential, and sedimental potential [9-12]. These forces have a critical influence on DNA translocation. DNA can be driven into nanostructures including nanopore, nanoslit, nanochannel by electrically applying pressure-driven flow [69-71]. To be specific, Based on the applied voltage to the electrodes, electroosmosis flow (EOF) or electrophoresis flow (EP) can be generated near the inlet of nanostructure towards the opposite way to DNA translocation. Thus, these two repellent forces disturb DNA molecules to come into the nanostructure for DNA sequencing. Besides, these two forces are also significantly affected by electrokinetic surface charge density of base polymers used as a substrate of nanofluidic devices [72]. Thus, when it comes to making an effective nanofluidic biosensor, it's crucial to have a material that has low electrokinetic surface charge density as well as robust mechanical and chemical stability.

For these properties, organic polymers have mainly been used for nanofluidic devices because organic polymer nanofluidic devices have a lower electrokinetic surface charge density than inorganic-based nanofluidic devices. In the recent past, Tons of nanolithography methods for polymer-based nanofluidic devices have been developed [53, 56]. Among those methods, ultraviolet (UV)-NIL has been established as one of the powerful methods. UV-NIL is the nanoimprint lithography method to utilize UV resist that can be solidified by UV light, instead of thermoplastic [54]. There are two general categories of UV-resin, Positive and negative photoresists. Positive photoresist becomes soluble upon the UV-light exposure because the molecular bindings between monomers are broken by UV-light, while negative

photoresist becomes insoluble due to the connected molecular bindings between monomers by UV-light.

One main benefit of using UV-resin as a mold is its excellent demolding property due to its low Young's modulus and low electrokinetic surface charge density [58]. Zheng et al investigated the effect of surface charge density for DNA translocation via polymer-based nanochannels (COC6013, PMMA, and PEGDA for a substrate and COC 8007 for a cover sheet) [59]. The first two are thermoplastics; to form the nanochannels, they are heated to above their glass transition temperatures (Tg) and compressed with a hot press. The third one is a UV curable resin. To form nanodevices, the liquid (PEGDA) UV resin is poured onto a PMMA backbone substrate with 175 μm thickness and cured with UV light. This can be used to make nanofluidic devices with a higher resolution than the thermoplastic. As mentioned before, PEGDA has a low electrokinetic surface charge density as shown in Figure 2.15. The advantages of the decent demolding property and low electrokinetic surface charge density made PEGDA the best material for making these devices. However, PEGDA has weak chemical stability for long-term electrical measurement and ultimately DNA sequencing. There are two ways to improve the chemical stability of PEGDA. The first one is using high molar weight PEGDA (> Mn 200). But, the electrokinetic surface charge density increases as the molar weight of PEGDA increases, which has a negative effect on DNA translocation. Thus, the second method can be utilizing a crosslinking agent to enhance this stability issue.

The crosslinking reaction leads to the formation of insoluble coatings, where polymer chains are joined together to form a three-dimensional network. Extensive crosslinking results in an insoluble and infusible network of linked polymer chains [60]. Covalent bonds are formed by suitable functional groups located on polymer binder molecules. Increasing the cross-linking agent such as trimethylolpropane triacrylate (TMPTA) (Figure 2.16), concentration in the resist composition has a positive effect on the chemical stability of nanofluidic devices [61].

Therefore, the crosslinking agent concentration in the resist is an important parameter that can affect the chemical and corrosion resistance and mechanical strength of UV resin. Chemical stability also plays an important role in determining the mechanical properties of the nanofluidic devices, such as mechanical strength and surface hardness. In general, materials with higher chemical stability will be stronger and have greater hardness. Increasing the strength and hardness helps avoid an undesirable process called the swelling effect, which is a phenomenon that the walls of the nanodevices absorb the solution in the channels and start to swell [62]. This dimension change of the nanostructures on the nanofluidic devices due to the swelling effect may lower the functionality of the device to translocate biomolecules into the nanostructures.

Crosslinking reactions between PEGDA and TMPTA increase the crystallinity of the PEGDA by serving as a bonding agent between PEGDA molecules (Figure 2.17) [63]. Higher crystallinity also implies higher mechanical strength and surface hardness; this was verified experimentally using PEGDA resin with different TMPTA concentrations. Experiments were conducted to validate the chemical and mechanical effects of TMPTA concentrations in PEGDA resins and to support the effects of TMPTA on surface charge density, DNA translocating ability, and the shrinkage of nanostructures.

In this paper, we describe the improvement of the chemical and mechanical stabilities of UV resin-based nanofluidic devices by adding a crosslinking agent (TMPTA). The crosslinking reaction between PEGDA and TMPTA increases the crystallinity of the PEGDA by serving as a bonding agent between PEGDA molecules. It makes the polymer more chemically stable and higher crystallinity is linked to higher mechanical strength and surface hardness. Experiments were conducted to validate the chemical and mechanical effects of TMPTA concentrations in PEGDA resins, and to support the effects of TMPTA on electrokinetic surface charge density and the shrinkage of nanostructures.

4.2. Experiment method

4.2.1 Materials and sample preparation

A silicon grating mold (MikroMasch) with 10μm pitch and 1μm height was used. The grating mold was replicated with MD700 UV-resin (Fluorolink PFPE, Solvay). It was then used as a final imprinting mold. PEGDA (Mn 200, Sigma-Aldrich) was used as a device material on a polyethylene terephthalate (PET) as a backbone substrate. The resin was composed of PEGDA as the base, different amounts of TMPTA (Sigma-Aldrich) as the cross-linking agent, and Irgacure 651 (Ciba) as a photoinitiator.

Five different compositions of PEGDA resins with varied amounts of crosslinking agent ,TMPTA, (pure PEGDA and PEGDA:TMPTA ratios of 5:1, 1:1, 1:2, and 1:5) were prepared. We performed this experiment on the flat surface. UV resins were exposed to UV light (365 nm) for 6 min at an intensity of 30 mW/cm2 and 5 min for post-curing after the demolding process. Three different TMPTA concentrations into PEGDA resin (pure PEGDA, PEGDA-TMPTA 1:1, and 1:5) were employed.

4.2.2 Nanoindentation hardness measurement

Nanoindentation hardness measurement was conducted on a Nanointenter XP system (MTS Systems Corp., Knoxville, TN), in a force-controlled mode with a maximum force of 40 mN and a force rate of 1 mN/sec. For each sample, at least 6 measurements were carried out, and the distance between every two adjacent points was set to be 50 μm. The depth of the resulting indentation was measured to obtain the relative hardness. Figure 4.1 shows the example of nanoindentation depth according to the load on the sample. The x-axis refers to the displacement which means the depth from the surface. The y-axis refers to the force loaded on the sample surface. The maximum depth of this experiment is under 4μm.

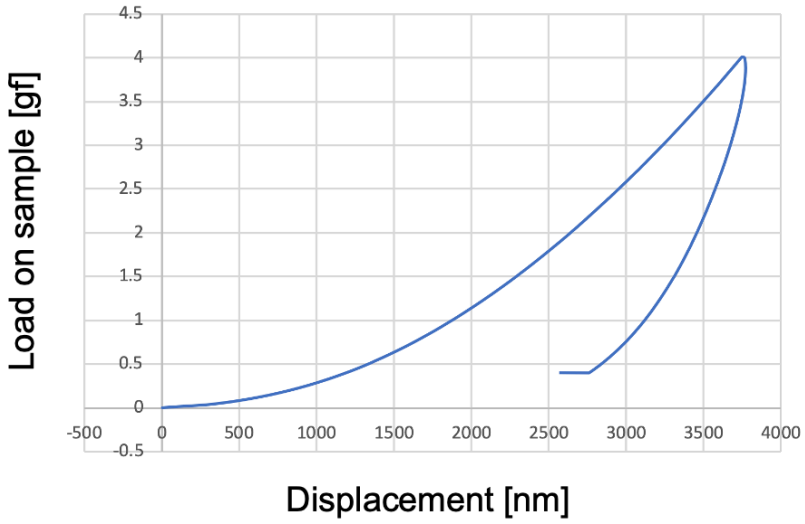

Figure 4.1. The plot of the nanoindentation depth according to the load on the sample.

Nanoindentation depth is required to be 10 times smaller than the entire sample thickness to exactly measure the surface hardness without other variables due to material properties, such as stiffness and tensile strength. Figure 4.2(a) illustrates the schematic figure of the PEGDA-TMPTA sample and Figure 4.2(b) is the index of the thickness of each PEGDA-TMPTA resin layer on the sample.

(a)

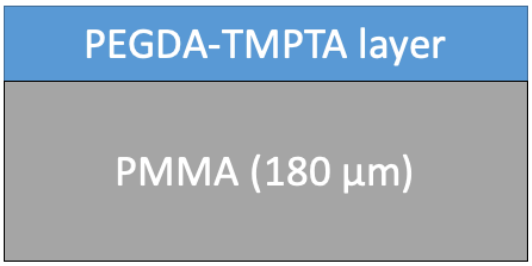

(b)

	Sample thickness
Pure PEGDA	54 µm
PEGDA-TMPTA 5:1	66 µm
PEGDA-TMPTA 2:1	73 µm
PEGDA-TMPTA 1:1	63 µm
PEGDA-TMPTA 1:2	60 µm
PEGDA-TMPTA 1:5	71 µm

Figure 4.2. Schematic figure of a PEGDA-TMPTA sample (a) and the thicknesses of PEGDA-TMPTA samples (b).

4.2.3 SEM measurement

We used 5μm width Si grating mold to check shrinkage according to the TMPTA concentration. We copied the grating pattern on the PEGDA-TMPTA resin and check the cross-sectional view after breaking down the sample. Figure 4.3 shows the SEM images of the pattern on the silicon grating mold. The dimension of the grating pattern is 10 μm in width, 1 μm in height, and 15 μm pitch.

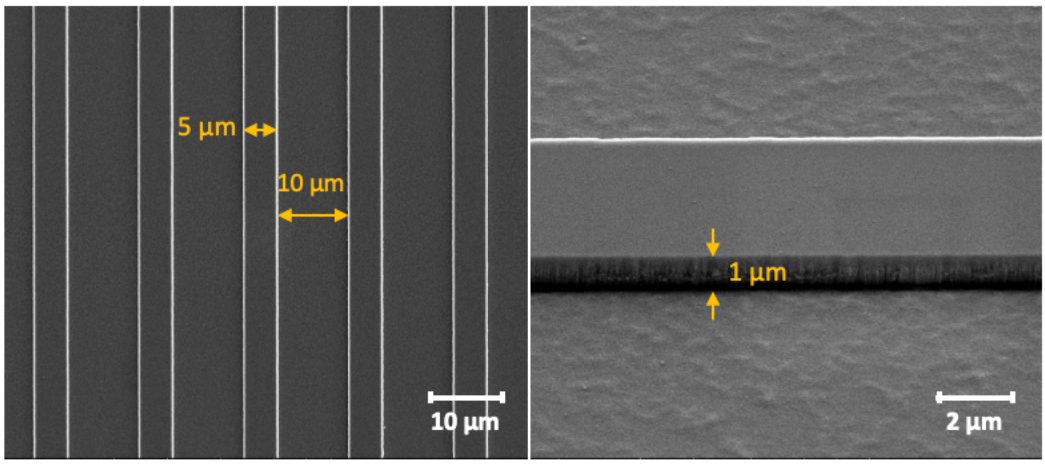

Figure 4.3. SEM images of 5 μm silicon grating mold.

Figure 4.4 describes the entire process of PEGDA-TMPTA sample preparation for checking the shrinkage of the cross-sectional area. We transferred the target pattern on the PEGDA-TMPTA resin by using the MD700 mold. We made a scratch to easily break down the PEGDA-TMPTA device after freezing it in the fridge. After then, the device is broken down into two pieces with a clear cross-section. We measure and compare the dimensions of the nanochannels on each concentration of PEGDA-TMPTA resins. Figure 4.5(a) shows the actual PEGDA-TMPTA samples and MD 700 mold. The direction of checking the cross-section view is shown in Figure 4.5(b).

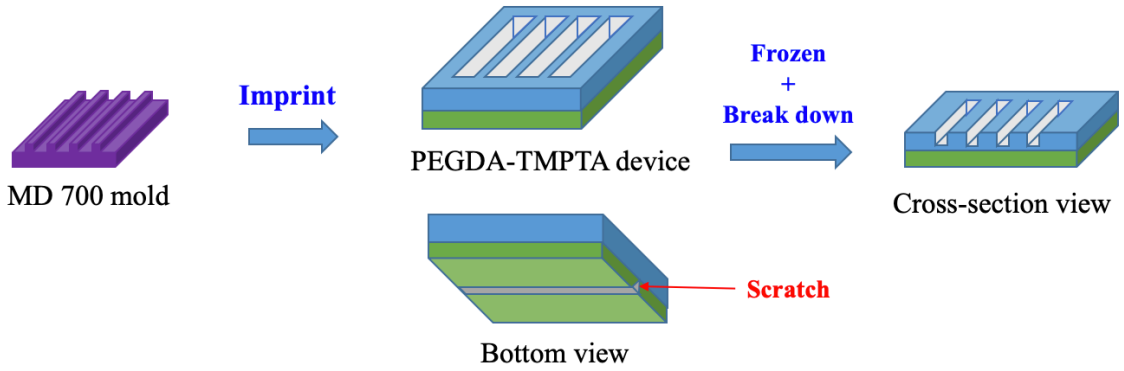

Figure 4.4. Schematic figure of the process to make the PEGDA-TMPTA samples for cross-section area.

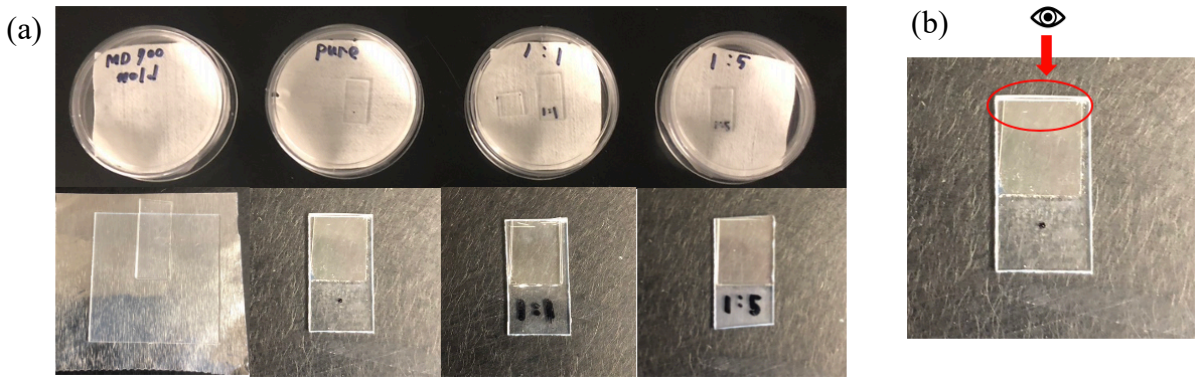

Figure 4.5. (a) Actual PEGDA-TMPTA samples and (b) the part for checking the cross-section area.

4.3. Result and Discussion

4.3.1 Nanoindentation hardness measurement

We measured the hardness of different PEGDA-TMPTA resins having varied amounts of crosslinking agent (pure PEGDA and PEGDA:TMPTA ratios of 5:1, 1:1, 1:2, and 1:5) to define the effect of the crosslinking agent composition on the hardness and ultimately on the swelling effect. The indentation depth was measured to obtain the relative hardness. This value is an indicator of the crystallinity of the PEGDA. Also, it is important because polymers with higher hardness and crystallinities will be less prone to the swelling effect.

The surface hardness of PEGDA-TMPTA resin increases according to the crosslinking agent concentration. The surface hardness of pure PEGDA was 0.139 GPa, 5:1 was 0.144 GPa, 2:1 was 0.158 GPa, 1:1 was 0.196 GPa, 1:2 was 0.204 GPa, and 1:5 was 0.205 GPa. The sample thicknesses were 54 µm, 66 µm, 73 µm, 63 µm, 60 µm, and 71 µm, respectively, in Figure 4.6.

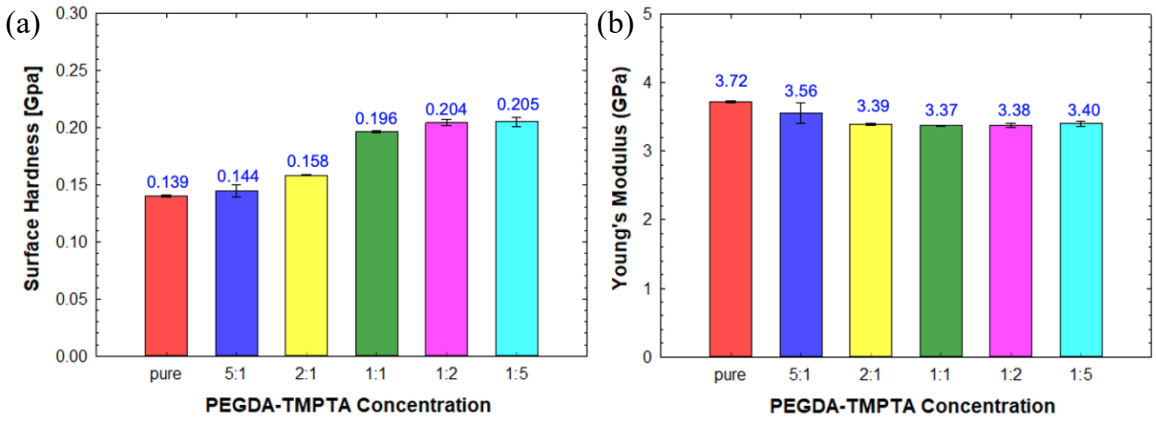

Figure 4.6. Surface Hardness (a) and young's modulus (b) of all PEGDA-TMPTA concentrations UV resins

The huge increase in the surface hardness occurs between 2:1 and 1:1. After the PEGDA-TMPTA composition of 1:1, the increase in the surface hardness is relatively reduced than before due to the increased crystallinity. To decide the optimized PEGDA-TMPTA composition for nanofluidic biosensors, we check the zeta-potential and surface charge density of each composition in the next part.

4.3.2 Zeta potential and electrokinetic surface charge density measurement

To optimize a material for nanofluidic devices, it is necessary to define the zeta-potential and electrokinetic surface charge density of each PEGDA-TMPTA based on the increase in the surface hardness according to the TMPTA concentration.

The zeta potentials for all five PEGDA-TMPTA samples are shown in Figure 4.7. The effect of TMPTA on zeta potential between pure PEGDA and PEGDA-TMPTA 1:1 is relatively more critical than between PEGDA-TMPTA 1:1 and PEGDA-TMPTA 1:5. Beyond PEGDA-TMPTA 1:1, the effect of TMPTA on zeta potential is trivial. The values between PEGDA-TMPTA 1:1 and PEGDA-TMPTA 1:5 within the error range of each of them. Adding TMPTA into PEGDA have a positive effect on changing zeta potential.

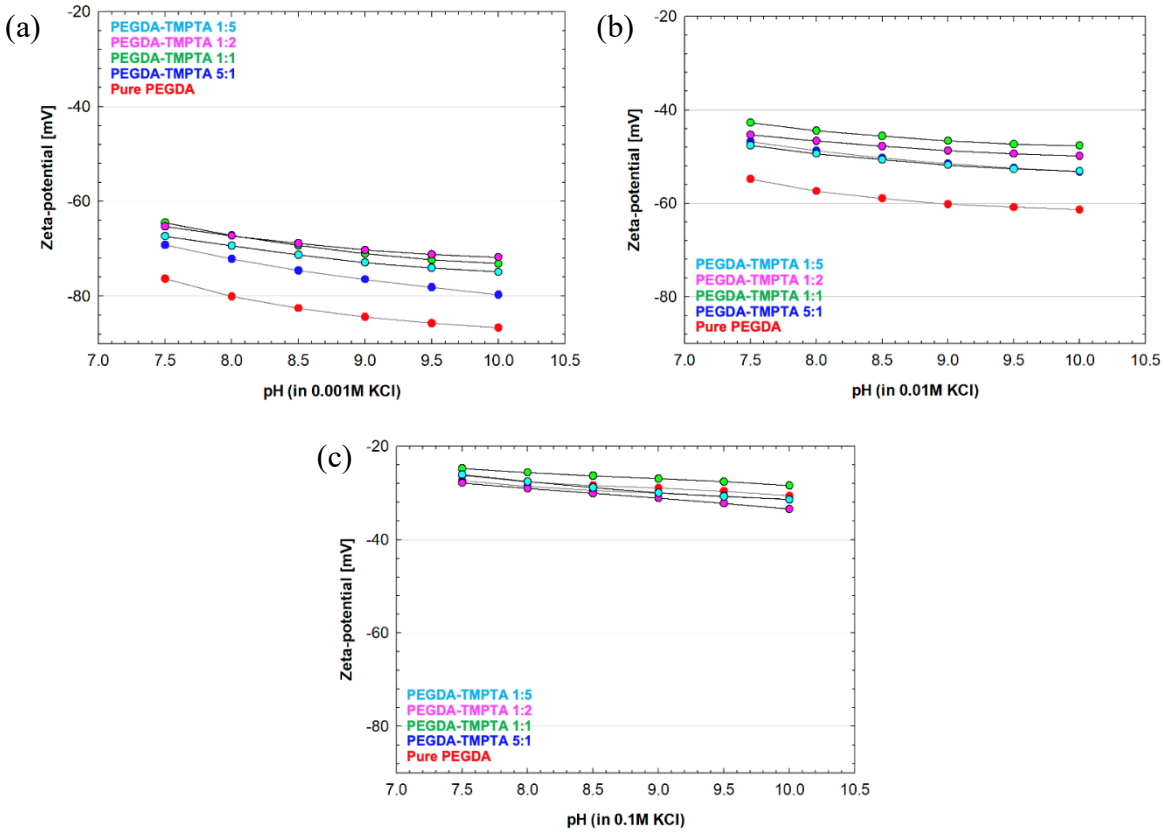

Figure 4.7. The result of zeta potential measurement for all five PEGDA-TMPTA samples: (a) in 0.001M KCl, (b) in 0.01M KCl, and (c) in 0.1M KCl.

Figure 4.8 indicates adding crosslinking-agent decreases electrokinetic surface charge density up to PEGDA-TMPTA 1:1 concentration from pure PEGDA concentration. The electrokinetic surface charge density between pH 7.5 and 10.5 of PEGDA-TMPTA resin slightly decreased from $-8.7 \sim -11.0\, mC/m^2$ for pure PEGDA resin to $-7.1 \sim -8.4\, mC/m^2$ for the ratio 1:5 resin. The hardness tends to increase as the TMPTA concentration increases, while young's modulus tends to decrease. The hardness relatively increases faster between pure PEGDA and 1:1 concentration than between 1:1 and 1:5 concentration. The effect of TMPTA on the hardness is more critical between pure PEGDA and 1:1 concentration, but the effect is comparably trivial beyond 1:1 up to 1:5 concentration.

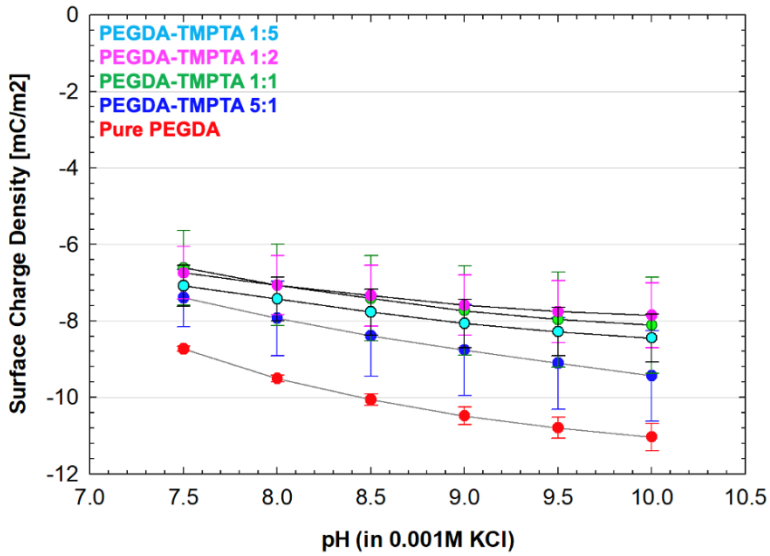

Figure 4.8. the plot of electrokinetic surface charge density between pH 7.5 and 10.5 of PEGDA-TMPTA in 0.001M KCl

4.3.3 Nanostructure dimension change measurement

The dimension is proportionally related to zeta-potential and electrokinetic surface charge density. Thus, it is necessary to investigate how much the dimension change occurs as TMPTA concentration increases for the optimization of the nanofluidic system. TMPTA which is the crosslinking agent functions as a bonding agent between PEGDA molecules. This bonding force generates the shrinkage of PEGDA as TMPTA concentration increases.

As shown in Figure 4.9, the cross-sectional view of the PEGDA-TMPTA devices can be checked by using an SEM to compare the dimensions of their nanochannels. The ability to directly check the nanochannel dimensions of the devices removes the need for creating a protrusive mold and using an AFM.

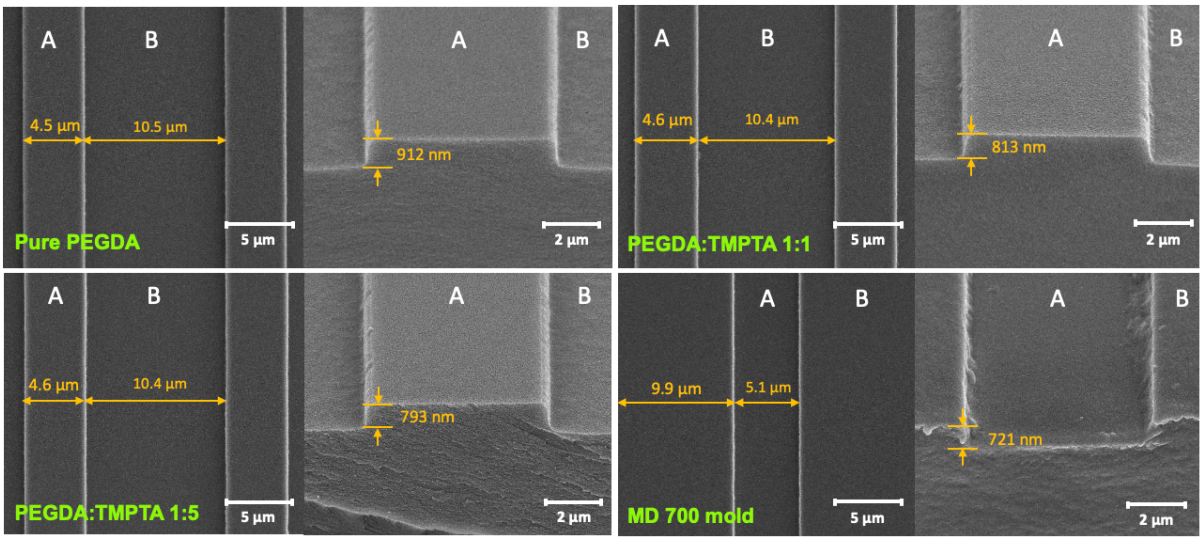

Figure 4.9. SEM images of a cross-section view of grating pattern on Pure PEGDA, PEGDA-TMPTA 1:1, PEGDA-TMPTA 1:5 resin, and MD 700 mold. The amount of cross-section areas decrease by 9.6% from pure PEGDA to PEGDA-TMPTA 1:1. The amount of cross-section areas decrease by 12.5 % from pure PEGDA to PEGDA-TMPTA 1:5.

The amount of cross-sectional area of nanochannels on the devices decreased by 9.6% from pure PEGDA to PEGDA:TMPTA 1:1 and by 12.5% from pure PEGDA to PEGDA:TMPTA 1:5. For pure PEGDA the width of (A) was 4.5 µm, the width of (B) was 10.5 µm, and the depth was 912 nm. For PEGDA:TMPTA 1:1 the width of (A) was 4.6 µm, the width of (B) was 10.4 µm, and the depth was 813 nm. For PEGDA:TMPTA 1:5 the width of (A) was 4.6 µm, the width of (B) was 10.4 µm, and the depth was 793 nm. For the MD 700 mold, the width of (A) was 9.9 µm, the width of (B) was 5.1 µm, and the depth was 721 nm. Figure 4.10 indicates the shirinkage rates functions of crosslinking agent contents.

(a)

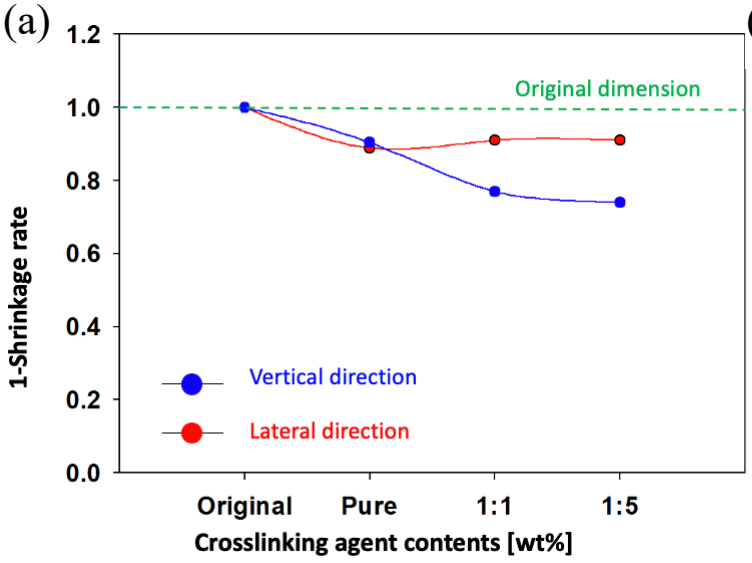

(b)

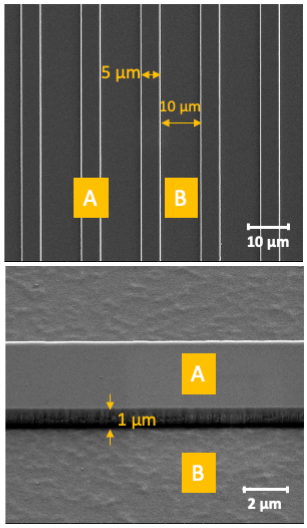

(c)

	A	Shrinkage rate	B	Shrinkage rate	Depth	Shrinkage rate
Silicon mold	5 µm	-	10 µm	-	1000 nm	-
MD 700 (Protrusive)	5.1 µm	0.020	9.9 µm	- 0.010	x	
Pure PEGDA	4.5 µm	- 0.111	10.5 µm	0.048	912 nm	- 0.096
PEGDA-TMPTA 1:1	4.6 µm	- 0.087	10.4 µm	0.038	813 nm	- 0.230
PEGDA-TMPTA 1:5	4.6 µm	- 0.087	10.4 µm	0.038	793 nm	- 0.261

Figure 4.10. Shrinkage rate of PEGDA-TMPTA resins: (a) plot of the 1-shrinkage rate versus crosslinking agent contents (wt%), (b) SEM image of silicon grating mold, and (c) shrinkage values of all PEGDA-TMPTA resins from the dimension of pattern on the silicon mold.

The calculated surface charge densities of the PEGDA-COC device without TMPTA and two PEGDA-COC devices with the PEGDA:TMPTA ratio 1:1 and 1:5 are $-16.8 \pm 1.95\ mC/m^2$, $-18.2 \pm 1.01\ mC/m^2$, and $-19.8 \pm 5.16\ mC/m^2$, respectively. Based on the SEM measurement result above, it is obvious that the shrinkage happens as TMPTA concentration increases. However, compared to the hardness improvement and device's chemical stability, this shrinkage issue would not have caused a remarkable phenomenon.

4.4. Conclusion

We studied the device stability of PEGDA plastic nanofluidic devices by incorporating crosslinking agent with different concentrations. the effects of the crosslinking agent is effective for improving the chemical and mechanical device stability without harmful drawbacks. To be specific, the effects of adding TMPTA to PEGDA on the zeta-potential, surface hardness, and electrokinetic surface charge density were much more significant when comparing a 1:1 composition to pure PEGDA than when comparing the 1:5 and 1:1 compositions. The amount of cross-section areas decrease by 9.6% from pure PEGDA to PEGDA-TMPTA 1:1 and also decrease by 12.5 % from pure PEGDA to PEGDA-TMPTA 1:5. In general, as the concentration of the salt solution increased, the zeta-potential of PEGDA-TMPTA samples decreased. Additionally, adding TMPTA to PEGDA had a positive effect on its electrokinetic surface charge density, tending to decrease its value for TMPTA concentrations up to 1:1. In its resin form, the material must fall within a range of viscosities that allows it to flow into the mold. The material must also have a low enough viscosity in its resin form to flow into the mold without defects. Several materials were used to find the best compromise between all these requirements. Based on this study, we can improve the chemical and mechanical stability of PEGDA devices, keeping low surface charge density.

CHAPTER 5. CONCLUSIONS AND FUTURE WORK

The result in Chapter 3 indicates an increase in zeta potential and surface roughness as the O_2 plasma treatment time increases. In each case, the untreated sample exhibited lower values than the 30s O_2 treated samples. The O_2 treatment increases roughness in the first 30s and continues to increase roughness with longer treatment times. This indicates that the charge drop created by the first 30 seconds of treatment was caused by the increase in surface roughness due to the O_2 treatment, and this unknown effect does not increase with treatment time. After 30 seconds of O_2 treatment, the surface roughness continues to increase with further O_2 treatment. This increased surface roughness causes a decrease in the velocity of the streaming current between the two samples in the cell. The reduced streaming current, in turn, decreases the zeta potential value due to their proportional relationship. Consequently, the electrokinetic surface charge density decreases based on the trend of zeta potential. Hence, it is possible to alter the electrokinetic surface charge density of materials by controlling their surface roughness and O_2 plasma treatment.

In Chapter 4, the effects of the crosslinking agent are obviously effective for improving the chemical and mechanical device stability without harmful drawbacks. To be specific, the effects of adding TMPTA to PEGDA on the zeta-potential, surface hardness, and electrokinetic surface charge density were much more significant when comparing a 1:1 composition to pure PEGDA than when comparing the 1:5 and 1:1 compositions. In general, as the concentration of the salt solution increased, the zeta-potential of PEGDA-TMPTA samples decreased. Additionally, adding TMPTA to PEGDA had a positive effect on its electrokinetic surface charge density, tending to decrease its value for TMPTA concentrations up to 1:1. In its resin form, the material must fall within a range of viscosities that allows it to flow into the mold. The material must also have a low enough viscosity in its resin form to flow into the mold without defects. Several materials were used to find the best compromise between all these

requirements. In conclusion, adding a crosslinking agent into PEGDA has a positive effect on the UV resin-based nanofluidic devices.

For the future work, We need to study the initial huge increase in the absolute value of zeta potential for polymers after 30 seconds O_2 plasma treatment. This phenomenon would be related to surface chemistry. We will come up with the method to measure accurate MD 700 mold cross-section area by using an atomic force microscope (AFM) . When we perform frozen cutting process for dimension checking, there was a difficulty to break the MD 700 samples and check accurate the cross-section area of MD 700 mold because of the flexibility of the backbone plates (PC). Plus, We will determine actual surface roughness of polymers after O_2 plasma treatment by using AFM. Lastly, we will investigate the functionality of PEGDA-TMPTA nanofluidic devices for NDA translocation by using a fluorescence microscopy.

Vita

Dae Won Kim was born and raised in Gumi, Korea. He was a professional Taekwondo player in middle school. After graduating High School from the Gyeonggu high school, he went to Sunmoon University in Cheonan, Korea where he completed his Bachelor of Science degree in Mechanical Engineering in Feb 2017. During the bachelor's degree, he served in the korean air force from 2011 to 2013 as a combat soldier. He had the honor of the best combat soldier in the Korean air force. He graduated from Sunmoon University and achieved scholarships; academic excellent scholarship 2014, 2015, and 2016; research foundation of Korea scholarship 2014. Upon graduating, he moved to Baton Rouge, Louisiana to pursue a Master of Science degree in Mechanical Engineering. He plans to pursue a career in research and development in nanoelectromechanical systems after the completion of his degree.

REFERENCES

1. Jameson, J.L. and D.L. Longo, *Precision medicine—personalized, problematic, and promising.* Obstetrical & gynecological survey, 2015. **70**(10): p. 612-614.
2. Hasnain, M.J.U., et al., *2. A review on nanopore sequencing technology, its applications and challenges.* Pure and Applied Biology (PAB), 2020. **9**(1): p. 154-161.
3. Hahm, J.-i., *Functional polymers in protein detection platforms: Optical, electrochemical, electrical, mass-sensitive, and magnetic biosensors.* Sensors, 2011. **11**(3): p. 3327-3355.
4. Prakash, S., M. Pinti, and B. Bhushan, *Theory, fabrication and applications of microfluidic and nanofluidic biosensors.* Philosophical Transactions of the Royal Society A: Mathematical, Physical and Engineering Sciences, 2012. **370**(1967): p. 2269-2303.
5. Feng, Y., et al., *Nanopore-based Fourth-generation DNA Sequencing Technology.* Genomics, Proteomics & Bioinformatics, 2015. **13**(1): p. 4-16.
6. Steveson, M. and K. Sagoe-Crentsil, *Relationships between composition, structure and strength of inorganic polymers.* Journal of materials science, 2005. **40**(8): p. 2023-2036.
7. Shaurya Prakash, J.Y., *Nanofluidics and microfluidics: systems and applications*. 2014, Elsevier: William Andrew.
8. Sparreboom, W., van den Berg, A. & Eijkel, J., *Principles and applications of nanofluidic transport.* Nature Nanotech, 2009. **4**: p. 713–720.
9. Squires, T.M. and M.Z. Bazant, *Induced-charge electro-osmosis.* Journal of Fluid Mechanics, 2004. **509**: p. 217-252.
10. Caballero, B., L.C. Trugo, and P.M. Finglas, *Encyclopedia of food sciences and nutrition*. 2003: Academic.

11. Revil, A., et al., *Streaming potential in porous media: 2. Theory and application to geothermal systems.* Journal of Geophysical Research: Solid Earth, 1999. **104**(B9): p. 20033-20048.

12. Marlow, B.J. and R.L. Rowell, *Sedimentation potential in aqueous electrolytes.* Langmuir, 1985. **1**(1): p. 83-90.

13. Lee, C.S., W.C. Blanchard, and C.T. Wu, *Direct control of the electroosmosis in capillary zone electrophoresis by using an external electric field.* Analytical Chemistry, 1990. **62**(14): p. 1550-1552.

14. Jorgenson, J.W. and K.D. Lukacs, *Capillary zone electrophoresis.* Science, 1983. **222**: p. 266-274.

15. Leung, V., et al., *Streaming potential sensing in paper-based microfluidic channels.* Colloids and Surfaces A: Physicochemical and Engineering Aspects, 2010. **364**(1-3): p. 16-18.

16. Saville, D., *The sedimentation potential in a dilute suspension.* Advances in Colloid and Interface Science, 1982. **16**(1): p. 267-279.

17. Chantiwas, R., Park, S., Soper, S.A., Kim, B.C., Takayama, S., Sunkara, V., Hwang, H. and Cho, Y.K., *Flexible fabrication and applications of polymer nanochannels and nanoslits.* Chemical Society Reviews, 2011. **40**(7): p. 3677-3702.

18. Zhou, K., J.M. Perry, and S.C. Jacobson, *Transport and Sensing in Nanofluidic Devices.* Annual Review of Analytical Chemistry, 2011. **4**(1): p. 321-341.

19. Squires, T.M., R.J. Messinger, and S.R. Manalis, *Making it stick: convection, reaction and diffusion in surface-based biosensors.* Nature Biotechnology, 2008. **26**(4): p. 417-426.

20. Schoch, R.B., L.F. Cheow, and J. Han, *Electrical detection of fast reaction kinetics in nanochannels with an induced flow.* Nano letters, 2007. **7**(12): p. 3895-3900.

21. Braus, M., *The theory of electrolytes. I. Freezing point depression and related phenomena (Translation).* 2019.

22. Uba, F.I., et al., *Surface charge, electroosmotic flow and DNA extension in chemically modified thermoplastic nanoslits and nanochannels.* Analyst, 2015. **140**(1): p. 113-126.

23. Plecis, A., R.B. Schoch, and P. Renaud, *Ionic transport phenomena in nanofluidics: experimental and theoretical study of the exclusion-enrichment effect on a chip.* Nano letters, 2005. **5**(6): p. 1147-1155.

24. Gu, Y. and D. Li, *The ζ-potential of glass surface in contact with aqueous solutions.* Journal of Colloid and Interface Science, 2000. **226**(2): p. 328-339.

25. Tandon, V., et al., *Zeta potential and electroosmotic mobility in microfluidic devices fabricated from hydrophobic polymers: 1. The origins of charge.* Electrophoresis, 2008. **29**(5): p. 1092-1101.

26. Sze, A., et al., *Zeta-potential measurement using the Smoluchowski equation and the slope of the current–time relationship in electroosmotic flow.* Journal of colloid and interface science, 2003. **261**(2): p. 402-410.

27. Lauga, E. and H.A. Stone, *Effective slip in pressure-driven Stokes flow.* Journal of Fluid Mechanics, 2003. **489**: p. 55-77.

28. Luxbacher, T., *The ZETA guide: Principles of the streaming potential technique.* Anton Paar GmbH: Graz, Austria, 2014.

29. Werner, C., R. Zimmermann, and T. Kratzmüller, *Streaming potential and streaming current measurements at planar solid/liquid interfaces for simultaneous determination of zeta potential and surface conductivity.* Colloids and Surfaces A: Physicochemical and Engineering Aspects, 2001. **192**(1-3): p. 205-213.

30. Fievet, P., et al., *Determining the ζ-potential of plane membranes from tangential streaming potential measurements: effect of the membrane body conductance.* Journal of Membrane Science, 2003. **226**(1-2): p. 227-236.

31. Jalil, A.H. and U. Pyell, *Quantification of zeta-potential and electrokinetic surface charge density for colloidal silica nanoparticles dependent on type and concentration of the counterion: probing the outer Helmholtz plane.* The Journal of Physical Chemistry C, 2018. **122**(8): p. 4437-4453.

32. Hunter, R.J., *Zeta potential in colloid science: principles and applications*. Vol. 2. 2013: Academic press.

33. Johnson, T.J., et al., *Laser modification of preformed polymer microchannels: application to reduce band broadening around turns subject to electrokinetic flow.* Analytical Chemistry, 2001. **73**(15): p. 3656-3661.

34. Kirby, B.J. and E.F. Hasselbrink Jr, *Zeta potential of microfluidic substrates: 1. Theory, experimental techniques, and effects on separations.* Electrophoresis, 2004. **25**(2): p. 187-202.

35. Kirby, B.J. and E.F. Hasselbrink Jr, *Zeta potential of microfluidic substrates: 2. Data for polymers.* Electrophoresis, 2004. **25**(2): p. 203-213.

36. Caslavska, J. and W. Thormann, *Electrophoretic separations in PMMA capillaries with uniform and discontinuous buffers.* Journal of Microcolumn Separations, 2001. **13**(2): p. 69-83.

37. Locascio, L.E., C.E. Perso, and C.S. Lee, *Measurement of electroosmotic flow in plastic imprinted microfluid devices and the effect of protein adsorption on flow rate.* Journal of chromatography A, 1999. **857**(1-2): p. 275-284.

38. Ross, D. and L.E. Locascio, *Effect of caged fluorescent dye on the electroosmotic mobility in microchannels.* Analytical chemistry, 2003. **75**(5): p. 1218-1220.

39. Soper, S.A., et al., *Surface modification of polymer-based microfluidic devices.* Analytica Chimica Acta, 2002. **470**(1): p. 87-99.

40. Henry, A.C., et al., *Surface modification of poly (methyl methacrylate) used in the fabrication of microanalytical devices.* Analytical chemistry, 2000. **72**(21): p. 5331-5337.

41. Liu, Y., et al., *Dynamic coating using polyelectrolyte multilayers for chemical control of electroosmotic flow in capillary electrophoresis microchips.* Analytical chemistry, 2000. **72**(24): p. 5939-5944.

42. Bianchi, F., et al., *Electroosmotic flow in composite microchannels and implications in microcapillary electrophoresis systems.* Analytical chemistry, 2001. **73**(4): p. 829-836.

43. Roberts, M.A., et al., *UV laser machined polymer substrates for the development of microdiagnostic systems.* Analytical chemistry, 1997. **69**(11): p. 2035-2042.

44. Johnson, T.J., D. Ross, and L.E. Locascio, *Rapid microfluidic mixing.* Analytical chemistry, 2002. **74**(1): p. 45-51.

45. Duffy, D.C., et al., *Rapid prototyping of microfluidic switches in poly (dimethyl siloxane) and their actuation by electro-osmotic flow.* Journal of Micromechanics and Microengineering, 1999. **9**(3): p. 211.

46. Ocvirk, G., et al., *Electrokinetic control of fluid flow in native poly (dimethylsiloxane) capillary electrophoresis devices.* ELECTROPHORESIS: An International Journal, 2000. **21**(1): p. 107-115.

47. Lacher, N.A., et al., *Comparison of the performance characteristics of poly (dimethylsiloxane) and Pyrex microchip electrophoresis devices for peptide separations.* Journal of chromatography A, 2003. **1004**(1-2): p. 225-235.

48. Badal, M.Y., et al., *Protein separation and surfactant control of electroosmotic flow in poly (dimethylsiloxane)-coated capillaries and microchips.* Journal of chromatography A, 2002. **947**(2): p. 277-286.

49. Wang, S.-C., C.E. Perso, and M.D. Morris, *Effects of alkaline hydrolysis and dynamic coating on the electroosmotic flow in polymeric microfabricated channels.* Analytical chemistry, 2000. **72**(7): p. 1704-1706.

50. Henry, A.C., et al., *Control of electroosmotic flow in laser-ablated and chemically modified hot imprinted poly (ethylene terephthalate glycol) microchannels.* Electrophoresis, 2002. **23**(5): p. 791-798.

51. Barker, S.L., et al., *Control of flow direction in microfluidic devices with polyelectrolyte multilayers.* Analytical chemistry, 2000. **72**(24): p. 5925-5929.

52. Duan, C., W. Wang, and Q. Xie, *Fabrication of nanofluidic devices.* Biomicrofluidics, 2013. **7**(2): p. 026501.

53. Schift, H., *Nanoimprint lithography: An old story in modern times? A review.* Journal of Vacuum Science & Technology B: Microelectronics and Nanometer Structures, 2008. **26**(2): p. 458.

54. Wu, J., et al., *Complete plastic nanofluidic devices for DNA analysis via direct imprinting with polymer stamps.* 2011. **11**(17): p. 2984.

55. Choi, J., Z. Jia, and S. Park, *Fabrication of polymeric dual-scale nanoimprint molds using a polymer stencil membrane.* Microelectronic engineering, 2018. **199**: p. 101-105.

56. Choi, J., et al., *Fabrication of perforated micro/nanopore membranes via a combination of nanoimprint lithography and pressed self-perfection process for size reduction.* Journal of nanoscience and nanotechnology, 2013. **13**(6): p. 4129-4133.

57. Haisma, J., et al., *Mold-assisted nanolithography: A process for reliable pattern replication.* Journal of Vacuum Science & Technology B: Microelectronics and Nanometer Structures Processing, Measurement, and Phenomena, 1996. **14**(6): p. 4124-4128.

58. Jia, Z., J. Choi, and S. Park, *Selection of UV-resins for nanostructured molds for thermal-NIL.* Nanotechnology, 2018. **29**(36): p. 365302.

59. Jia, Z., J. Choi, and S. Park, *Surface Charge Density-Dependent DNA Capture through Polymer Planar Nanopores.* ACS applied materials & interfaces, 2018. **10**(47): p. 40927-40937.

60. Chattopadhyay, D., S.S. Panda, and K. Raju, *Thermal and mechanical properties of epoxy acrylate/methacrylates UV cured coatings.* Progress in Organic Coatings, 2005. **54**(1): p. 10-19.

61. Joo, H.-S., et al., *Adhesion performance of UV-cured semi-IPN structure acrylic pressure sensitive adhesives.* Journal of adhesion science and technology, 2006. **20**(14): p. 1573-1594.

62. Caldorera-Moore, M., et al., *Swelling behavior of nanoscale, shape-and size-specific, hydrogel particles fabricated using imprint lithography.* Soft Matter, 2011. **7**(6): p. 2879-2887.

63. Yang, W., et al., *Rapid fabrication of hydrogel microstructures using UV-induced projection printing.* Micromachines, 2015. **6**(12): p. 1903-1913.

64. Cheng, E., et al., *Surface modification-assisted bonding of 2D polymer-based nanofluidic devices.* Microfluidics and Nanofluidics, 2015. **18**(3): p. 527-535.

65. Schnitzer, C. and S. Ripperger, *Influence of Surface Roughness on Streaming Potential Method.* Chemical Engineering & Technology, 2008. **31**(11): p. 1696-1700.

66. Chai, J., et al., *Wettability interpretation of oxygen plasma modified poly (methyl methacrylate).* Langmuir, 2004. **20**(25): p. 10919-10927.

67. O'Neil, C.E., et al., *Characterization of activated cyclic olefin copolymer: effects of ethylene/norbornene content on the physiochemical properties.* Analyst, 2016. **141**(24): p. 6521-6532.

68. Anton-Paar, *The Zeta Potential as an Indicator of Surface Properties.*

69. Keyser, U.F., S. Van Dorp, and S.G. Lemay, *Tether forces in DNAelectrophoresis.* Chem. Soc. Rev., 2010. **39**(3): p. 939-947.

70. Menard, L.D. and J.M. Ramsey, *Electrokinetically-Driven Transport of DNA through Focused Ion Beam Milled Nanofluidic Channels.* Analytical Chemistry, 2013. **85**(2): p. 1146-1153.

71. Pennathur, S., et al., *Free-Solution Oligonucleotide Separation in Nanoscale Channels.* 2007. **79**(21): p. 8316-8322.

72. Rezaei, M., A.R. Azimian, and D.T. Semiromi, *The surface charge density effect on the electro-osmotic flow in a nanochannel: a molecular dynamics study.* 2015. **51**(5): p. 661-670.